RESEARCH ARTICLE

Basin Research   EAGE WILEY

Luminescence signals of quartz and feldspar as new methods for stratigraphic discrimination and provenance analysis of siliciclastic successions: The case of the Parnaíba Basin (Brazil) of West Gondwana

Ian del Río[1] | **André O. Sawakuchi[1]** | **Ana M. Góes[1]** |
Maria Helena B. M. Hollanda[1] | **Laura Y. Furukawa[1]** | **Naomi Porat[2]** |
Mayank Jain[3] | **Thays D. Mineli[1]** | **Francisco de Assis Negri[4]**

[1]Instituto de Geociências, Universidade de São Paulo, São Paulo, Brazil

[2]Geological Survey of Israel, Jerusalem, Israel

[3]Department of Physics, Technical University of Denmark, Roskilde, Denmark

[4]Secretaria de Infraestrutura e Meio Ambiente do Estado de São Paulo, Instituto Geológico, São Paulo, Brazil

Correspondence
Ian del Río, Instituto de Geociências, Universidade de São Paulo, Rua do Lago, 562, 05508-080, São Paulo, SP, Brazil. Email: iandelrio@usp.br

Funding information
Conselho Nacional de Desenvolvimento Científico e Tecnológico, Grant/Award Number: 303201/2019-3 and 304727/2017-2; FAPESP, Grant/Award Number: 2019/20588-9; Petrobras/ANP: 0050.0069726.11.9

Abstract

Luminescence characteristics of quartz and feldspar allow to discriminate sediments from different source areas. Particularly, sensitivity of optically stimulated luminescence (OSL) and thermoluminescence (TL) signals of quartz and infrared-stimulated luminescence (IRSL) of feldspar from Quaternary sediments has been used for provenance analysis. These properties change due to source area denudation rates and sediment reworking, which drive the number of burial irradiation-solar exposure cycles of sediment grains in surface systems. Here, we use for the first time a similar approach to interpret the geomorphic conditions of source areas of Silurian to Triassic siliciclastic sedimentary units of the intracratonic Parnaíba Basin in northeast Brazil. Luminescence measurements were performed on sand grains, and statistical tests were applied to evaluate differences in luminescence properties within and across stratigraphic units. We explored the position of well-known "110°C" (TL_{110}) and "325°C" (TL_{325}) TL peaks of quartz as proxies to discriminate stratigraphic units with similar lithological assemblages. OSL and TL sensitivities as well as the dominance of the so-called fast OSL component increase from Silurian to Triassic sedimentary units, while the IRSL sensitivity decreases towards younger stratigraphic units. These patterns point to source areas with decreasing denudation rate and higher sediment recycling over basin filling time, leading to decreasing feldspar concentration and quartz luminescence sensitisation. Major changes in luminescence properties coincide with regional unconformities. This is attributed to physical landscape changes leading to shifts in the relief of source areas and basin sediment recycling. The TL_{110} peak position is similar across stratigraphic units, but the TL_{325} peak position has significant variation, with values between 324°C and 334°C, allowing its use for stratigraphic discrimination. Changes in OSL and TL characteristics of quartz sediment grains are preserved during long-term burial (10^8 Ma), representing a new

tool for interpreting basin evolution and to perform stratigraphic analysis of ancient siliciclastic successions.

1 | INTRODUCTION

Ionising radiation reaching minerals creates free electrons in the crystal lattice of quartz and feldspar grains. The free electrons and their counterparts, named holes, are subsequently captured in defects (traps) within the crystal lattice (Wintle & Adamiec, 2017). When quartz or feldspar grains are stimulated by heat or light, these electrons evict from their traps and recombine with the holes, when photons can be emitted (Bailey, 2001). When the grain is stimulated by heat, the process is called thermoluminescence (TL) whereas optically stimulated luminescence (OSL) names the process when the stimulation is visible light and infrared stimulated luminescence (IRSL) is used when infrared stimulation is applied. OSL and TL occur both in quartz and feldspar while IRSL emission is typical of feldspar (Aitken, 1985). The TL, OSL and IRSL signals have been crucial in the development of dating methods applied to Quaternary sediments (Aitken, 1998; Murray & Wintle, 2000). More recently, the OSL and TL characteristics of quartz sediment grains have been used to track sediment transport in Quaternary systems (Gray et al., 2019). This includes the use of OSL and TL sensitivities (light emitted per unit mass per radiation dose) of quartz for sediment provenance analysis (Mendes et al., 2019; Zular et al., 2015).

Laboratory experiments demonstrate that repeating cycles of irradiation (trap filling) and illumination (charge eviction) promote the OSL sensitisation of quartz (Moska & Murray, 2006). In nature, the OSL sensitivity of quartz crystals in igneous and metamorphic rocks is generally low while the OSL sensitivity of quartz from Quaternary sediments has been observed to vary within four to five orders of magnitude (Sawakuchi et al., 2011, 2020). This suggests that the OSL sensitisation in nature is related to surface processes occurring after quartz crystals are released from their primary source rocks. These processes can include burial (irradiation) and surface exposure (sunlight stimulation) cycles during sediment transport (Pietsch et al., 2008; Sawakuchi et al., 2011) and soil reworking by bioturbation (Gray et al., 2017, 2019, 2020; Reimann et al., 2017). Both sediment transport and soil bioturbation would link OSL sensitisation to denudation rates of sediment source areas, where lower denudation rate leads to longer residence of quartz grains in soil and then, higher sensitisation (Sawakuchi et al., 2018). The OSL sensitivity of quartz in sediments is mirrored by the

Highlights

- Luminescence sensitivity is tested as a provenance proxy in sandstones of the Parnaíba Basin.
- Optically stimulated luminescence (OSL) and thermoluminescence (TL) sensitisation of quartz due to burial-solar exposure cycles is preserved after long-term burial.
- OSL sensitivity and the position of the "325°C" TL peak allow to discriminate stratigraphic units separated by unconformities.
- OSL signals indicate higher sediment recycling during the Carboniferous-Early Triassic.

IRSL/OSL ratio, which denotes the feldspar-to-quartz ratio (Sawakuchi et al., 2018). The OSL sensitisation of quartz by surface processes such as burial-exposure cycles would also be preserved in the subsurface temperature range typical of sedimentary basins (<200°C), suggesting that luminescence sensitivity may also be applied to study the sediment sources and transport conditions of ancient sedimentary successions. In this case, luminescence could lead to the development of provenance analysis method applied to ubiquitous minerals from siliciclastic rocks such as quartz and feldspar. This approach would be complimentary to well-established provenance analysis methods applied to sandy sediments such as U-Pb dating on detrital zircon grains (Fedo et al., 2003) and heavy mineral analysis (Morton & Hallsworth, 1999). Though both techniques have been largely improved over the years, provenance analysis by the use of accessory minerals from sedimentary rocks is still expensive and time consuming and depends on relatively large samples for heavy mineral concentration. As quartz and feldspar are the most abundant minerals in sandstones, the provenance and sedimentary transport conditions analysis based on their luminescence signals would be advantageous.

In this research, we explore the potential use of luminescence signals of quartz and feldspar to discriminate sedimentary units of the intracratonic Parnaíba Basin (Figure 1) and to reconstruct provenance changes during basin filling. The Parnaíba Basin, in northeast Brazi, (Vaz et al., 2007)
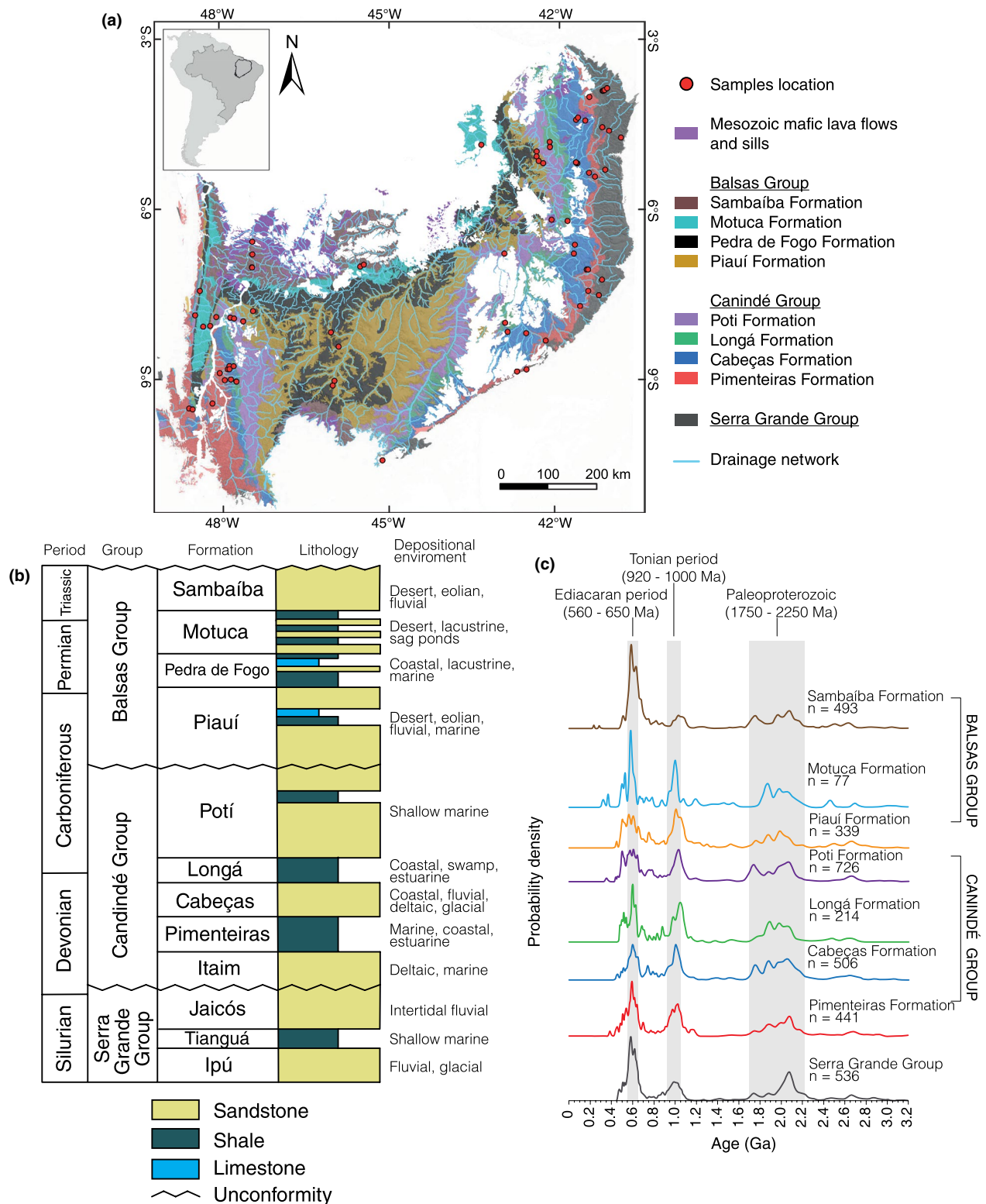
FIGURE 1 (a) Geological map of the Parnaíba Basin (Angelim et al., 2004; Vasconcelos et al., 2004) showing the location of the studied samples. (b) Simplified stratigraphic column representing the studied lithostratigraphic units and their interpreted depositional systems. Modified from Vaz et al. (2007) and Jaju et al. (2018). (c) Density plots of detrital zircon U/Pb ages from Hollanda et al. (2014)

hosts sedimentary successions ranging from the Silurian (ca. 444 Ma) to Triassic (ca. 201 Ma) and records diverse continental to marine depositional systems and a subsidence and

uplift history of around 200 Ma (Menzies et al., 2018; Tozer et al., 2017). This basin was also selected given its economic relevance for onshore gas production from sandstone reservoirs

(ANP, 2021). Previous provenance studies showed high similarity of detrital zircon ages of Parnaíba Basin sedimentary succession (Hollanda et al., 2014, 2018; Figure 1). Having this in mind, we developed a new application of luminescence signals from ancient sandstone samples for provenance analysis trying to minimise sample preparation, rapidness of measurement, and reducing laboratory equipment time. For this, we tested several luminescence characteristics of quartz and feldspar to: (a) discriminate between stratigraphic units hosting similar lithological assemblages; and (b) reconstruct landscape conditions during the basin filling period from the Silurian to the Triassic, such as source area denudation intensity, similar to the approach used by Sawakuchi et al. (2018) for Quaternary sediments. The measured luminescence characteristics are represented by the OSL and TL sensitivities and the peak positions of the well-known 110°C and 325°C TL peaks of quartz (Aitken, 1985) and the IRSL signal from feldspar. The obtained patterns of variation of the luminescence characteristics are discussed in terms of independent provenance indicators and changes of depositional systems during basin filling, as well as in terms of the tectonic conditions interpreted for the Parnaíba Basin evolution.

2 | GEOLOGICAL BACKGROUND

The Parnaíba Basin (Figure 1a), located in northeast Brazil, has a cratonic sag phase developed mainly during the Paleozoic over Precambrian rocks of the Amazon, São Luís and São Francisco cratons and the Borborema and Tocantins provinces (Cordani et al., 2009). The stratigraphic record of the basin is mostly composed of siliciclastic sediments deposited from the Silurian to the Triassic that can be divided into three lithostratigraphic Groups separated by regional unconformities (Vaz et al., 2007). Overall, the sedimentary sequences record an evolution from temperate to arid climate conditions, showing repetitive transgressive-to-regressive cycles (Góes & Feijó, 1994).

The lower-most sedimentary succession (Figure 1b) is represented by the Serra Grande Group, which comprises the Ipu, Tianguá and Jaicós Formations, ranging from Llandovery (Early Silurian) to Pragian (Early Devonian) (Grahn & Caputo, 1992; Grahn et al., 2005). The Serra Grande Group is overlain by the Canindé Group, comprising the Itaim, Pimenteiras, Cabeças, Longá and Potí Formations, from the Late Eifelian (Middle Devonian) to the Visean (Mississipian) (Góes et al., 1997; Grahn et al., 2008; Loboziak et al., 1992; Melo & Loboziak, 2000; Ponciano & Fávera, 2009; Ponciano et al., 2012). The Balsas Group represents the upper part of the sedimentary succession and encompasses sediments from the Piauí, Pedra de Fogo, Motuca, and Sambaíba Formations with ages from Late Bashkrian (Pennsylvanian) to the Late Triassic (Abrantes & Nogueira, 2013; Abrantes et al., 2016;

Araújo et al., 2016; Campanha & Rocha Campos, 1979; Cisneros et al., 2015; Medeiros, 2020; Medeiros et al., 2019; Vieira & Scherer, 2017).

After the cratonic sag phase, several volcanic events related to the opening of the Central and South Atlantic Ocean took place during the Early Cretaceous (Góes et al., 1993). This was followed by another episode of subsidence related to the South Atlantic opening (Rossetti et al., 2004). A series of inversion events between the Late Cretaceous-Neogene due to magmatic underplating and isostatic adjustment uplifted the basin until reaching its final configuration (Morais-Neto et al., 2009; Richetti et al., 2018).

Detrital zircon dating on sandstones from the aforementioned stratigraphic units yielded ages clustering at three main peaks of 1.75–2.75, 0.92–1.00 and 0.55–0.65 Ga (Hollanda et al., 2014; Figure 1c). The distribution of ages was homogeneous for all units, with the exception of the Sambaíba Formation which produced a higher density population of younger ages (0.55–0.65 Ga), attributed to sediments from Ediacaran rocks.

3 | BASIC CONCEPTS ON TL AND OSL OF QUARTZ AND FELDSPAR

Electron and hole traps are formed by defects in the crystal lattice of quartz and feldspar. These defects act as traps of charges and can be related to the substitution (impurity) or absence (vacancy) of elements forming the crystal lattice of quartz or feldspar. In quartz, the substitution of silicon by aluminum or the absence of oxygen in a crystal lattice position respectively represents defects related to impurity and vacancy (Preusser et al., 2009). Quartz OSL and TL signals arise from discrete traps, each one characterised by its own energy depth (Bailey, 2001). The differences in trap energy imply that when a quartz sample is progressively heated, the TL glow curve displays a number of light emission peaks, each arising from a different trap, typically located at temperature ranges of 90–110°C, 220–250°C and 325–375°C with the exact temperature depending on the heating rate (Chen & Li, 2000; Kitis et al., 2010). In the same way, the OSL signals also contain information about several electron-hole traps in a composite single decay curve (Jain et al., 2003). In order to access the trap information, it is needed to deconvolute the signal into a number of OSL components. For three OSL components, the deconvolution is performed following Equation 1 (Bøtter-Jensen et al., 2003):

$$I_{\text{OSL}(t)} = n_1 p_1 \exp^{-tp_1} + n_2 p_2 \exp^{-tp_2} + n_3 p_3 \exp^{-tp_3} \quad (1)$$

where I_{OSL} is the OSL intensity, $n_{1,2,3}$ is the initial concentration of trapped electrons in m^{-3}, $p_{1,2,3}$ is the rate of stimulation in s^{-1}, and t is the time of stimulation in s. The proportion of

OSL components and the position of the TL peaks of quartz along with their number and intensity has been showed to be sample dependent (Jain et al., 2003; Mineli et al., 2021; Rink et al., 1993). However, the relationship between TL peaks and OSL signals is not straightforward. The TL peak located at 110°C seems to be produced by a trap related to the production of the bulk OSL signal (Wintle & Murray, 1997). However, the bulk OSL signal has also been related to TL peaks located at ca. 325°C (Kitis et al., 2010).

Charges are trapped when quartz or feldspar grains are under burial irradiation and the luminescence signals arising from charge recombination due to stimulation by heating or light have varying stability. Charges trapped in low energy depths can present unstable behaviours, showing spontaneous loss and fading of their related signals over time or having short lifetimes when exposed to relatively low ambient temperatures (30–50°C) for long periods of time ($>10^4$–10^6 years). For instance, the quartz TL peak located at 110°C is highly unstable and entirely disappears after few hours at ambient temperature (Spooner & Questiaux, 2000). The observation of the quartz TL peak at 110°C is only possible if the heating stimulation is performed shortly after irradiation in the laboratory. OSL components of quartz also present variable thermal stabilities from weeks to over 10^9 years (Singarayer & Bailey, 2003). Hence, luminescence signals originating from stable trapped charges can be observed from natural radiation doses while unstable signals need to be regenerated by laboratory irradiation.

The eviction of charges from traps by light stimulation, leading to the reset of OSL or IRSL, is named "bleaching" (Singarayer et al., 2005). The light exposure time needed for complete bleaching also varies among luminescence signals from quartz or feldspar. Quartz OSL signals decay relatively quickly when exposed to light, only needing a few seconds of exposure to sun light to complete bleaching. However, some TL signals, especially those located at higher temperatures (>300°C) can be present even after days of light exposure (Spooner et al., 1988). Several laboratory experiments have demonstrated that both OSL and TL signals can be sensitised when quartz is exposed to sequential cycles of irradiation and bleaching (Lü & Sun, 2011; Moska & Murray, 2006).

In the case of feldspar, recent findings have suggested that the electron-hole traps are located along a continuum of energy depths (Jain & Ankjaergaard, 2011), thus producing an IRSL decay curve composed of a single component and a TL glow curve containing generally a single peak located between 150°C and 250°C, with a tail towards higher temperatures. In terms of signal stability, most IRSL signals show a constant athermal loss of signal with time, commonly known as fading (Kars et al., 2008; Thomsen et al., 2008, 2011). Contrary to quartz OSL signals, feldspar IRSL signals need longer exposures to light to reset, varying from few seconds to days. The compositional variations among feldspar results in different luminescence behaviours for K-feldspar, Na-feldspar, and plagioclase (Blair et al., 2005). For example, fading rates from feldspars appear to increase with increasing Ca content (Huntley & Lian, 2006; Valla et al., 2016). However, the relation between composition and resulting IRSL signals is not well constrained so far.

It is possible to describe the luminescence properties of a sediment sample using quartz and feldspar luminescence signals regenerated in laboratory. This approach has been used to track sediment transport and infer sediment sources (Gray et al., 2019; Sawakuchi et al., 2018). For this purpose, we highlight quartz OSL or TL sensitivities (light intensity emitted per unit mass and radiation dose), which increase when quartz grains experience repeated cycles of burial (irradiation) and solar exposure (bleaching) during soil development or sediment transport (Lü & Sun, 2011; Sawakuchi et al., 2018). Besides calculation of OSL or TL sensitivity as the light emission per unit mass and dose, the sensitivity can also be represented as the ratio or percentage of a given OSL component or TL peak in relation to the light emission of the total OSL decay or TL glow curves. For example, in highly recycled sediments (Pietsch et al., 2008), grains from soils with high reworking rates (Gray et al., 2017, 2020; Reimann et al., 2017), or sediments derived from settings with low denudation rates, typical OSL sensitivity values (first second of light emission) vary from 30% to 70%, while for sediments recently exhumed from igneous or metamorphic rocks from orogens such as the Andes Cordillera, OSL sensitivity values range from 5% to 20% (Sawakuchi et al., 2018).

4 | MATERIALS AND METHODS

Because of the difficulty in differentiating stratigraphic units using their detrital zircon ages (Hollanda et al., 2014), which rely on the presence of sedimentary rocks containing such minerals, we selected sandstone samples from the aforementioned units, with exception of the Pedra de Fogo and Itaim Formations due to lack of suitable samples for luminescence measurements. Additionally, the Serra Grande Group (Figure 1) was treated as a single stratigraphic unit since the identification of individual formations were not considered during sampling. In order to avoid possible thermal effects on OSL sensitivity, all samples were collected over more than 50 m of distance from any Mesozoic magmatic body (Figure 1).

In total, 82 samples from the Serra Grande Group ($n = 13$), Pimenteiras ($n = 9$), Cabeças ($n = 15$), Longá ($n = 9$), Potí ($n = 14$), Piauí ($n = 9$), Motuca ($n = 5$) and Sambaíba ($n = 8$) Formations were collected in outcrops distributed across the Parnaíba Basin (Figure 1). Sample preparation was performed under daylight and artificial light conditions. Samples were manually disaggregated and sieved, selecting

the 62–125 μm grain size fraction. The target sand fraction was then treated with concentrated H_2O_2 followed by $C_2H_2O_4$ at 5% to eliminate organic matter and iron oxides, respectively. The sand grains concentrates are referred as polymineralic, but they are composed mainly of quartz and feldspar. In this way, luminescence signals from quartz were measured in presence of feldspar. Despite their relatively low concentration in sandy sediments, main heavy minerals occurring in the studied samples (zircon, tourmaline, and rutile; Hollanda et al., 2014) also have low luminescence signal in comparison to quartz (Sawakuchi et al., 2020). The approach to measure polymineralic aliquots was used to simplify sample preparation procedures and allow luminescence measurements indicative of sand mineral composition (quartz-to-feldspar ratio). Feldspar content for selected samples (BP100, BP105, BP107 and BP114) was estimated by optical microscopy of thin sections, resulting in maximum contents of 15%.

Luminescence measurements were performed in the Luminescence and Gamma Spectrometry Laboratory at the Institute of Geosciences of the University of São Paulo using a Risø TL/OSL DA-20 reader equipped with a built-in beta source (^{90}Sr/^{90}Y; dose rate of 0.108 Gy/s for cups), a bialkali PM tube (Thorn EMI 9635QB), a sample heater plate, and blue and infrared light emitting diodes (LEDs). Luminescence signals (TL, OSL and IRSL) were detected through a 7.5 mm Hoya U-340 glass filter (290–340 nm).

Measurement procedures (Table 1) were designed to measure a variety of luminescence signals and parameters. Four aliquots were measured for each sample. The aliquots were standardised by volume using an acrylic plate with a microhole (150–200 grains) to minimise aliquot size effects (see procedure and aliquot mass estimate in Sawakuchi et al., 2018). The first step (Table 1) aimed to fully bleach the natural OSL signals. This was followed by a small beta dose (step 2) and a preheat (step 3). An infrared stimulation (step 4) was used to record the luminescence from feldspars and reduce their contribution to the OSL signal measured at step 5, aiming to record a signal dominated by quartz. Step

6 measured a remnant natural TL signal with an additive dose of 10 Gy (step 2) and after a preheat at 240°C (step 3). After an additional 10 Gy dose (step 7), a regenerated TL signal was measured (step 8). Step 9 aimed to measure the TL background.

OSL sensitivity ($\%BOSL_{1s}$) was calculated using the first second of light emission ($BOSL_{[step\ 5;\ 0-1s]}$) with background subtraction using the last 10 s ($BOSL\ BG_{[step\ 5;\ 90-100s]}$) (Figure 2a). The $\%BOSL_{1s}$ was calculated as the fraction of the $BOSL_{[step\ 5;\ 0-1s]}$ with respect to the integration of the whole (0–100 s) OSL decay curve ($BOSL_{[step\ 5;\ 0-100s]}$) after also subtracting the last 10 s for background removal ($BOSL\ BG_{[step\ 5;\ 90-100s]}$; Equation 2). The OSL decay curve was deconvoluted to isolate the contributions from the fast ($BOSL_F$), medium ($BOSL_M$), and slow ($BOSL_S$) OSL components in relation to the total $BOSL_{1s}$. Deconvolution was performed using the Fit_CWCurve function from the R package Luminescence (Kreutzer et al., 2021) based on Equation 1 (Bøtter-Jensen et al., 2003). The luminescence signal from feldspar was also assessed by the first 1.2 s of IRSL decay curve ($IRSL_{[step\ 4;\ 0-1.2s]}$) and the last 10 s as background ($IRSL\ BG_{[step\ 4;\ 90-100s]}$). This signal from feldspar is presented as the proportion of $IRSL_{1.2s}$ to $BOSL_{1s}$ ($\%IRSL_{1.2s}/BOSL_{1s}$; Equation 3).

Regarding TL signals, both sensitivity and peak positions of the named 110°C and 325°C TL peaks (Chen & Li, 2000; Kitis et al., 2010) were analysed. The sensitivity of the TL 110°C peak ($\%TL_{110°C}$) was estimated by integrating the TL glow curve between 80°C and 120°C ($TL_{[step\ 8;\ 80-120°C]}$) minus the background ($TL\ BG_{[step\ 9;\ 80-120°C]}$) in relation to the total TL glow curve ($TL_{[step\ 8;\ 0-450°C]}$) minus the total background ($TL\ BG_{[step\ 9;\ 0-450°C]}$; Equation 4, Figure 2b). Before regenerating this TL signal, another 10 Gy dose was given (step 7). The peak positions of the 110°C (TL_{110pos}) and 325°C (TL_{325pos}) TL peaks were estimated from the maximum TL intensity in the temperature range encompassing these peaks (steps 8 and 6 in Table 1, respectively). Though the samples were collected and prepared under sunlight and artificial

TABLE 1 Sequence of procedures used in luminescence measurements. Heating rate is 5°C/s in all cases

| Step	Procedure	Observations
1	Blue LEDs stimulation at 125°C for 100 s	
2	Dose, 10 Gy	
3	Preheat at 240°C for 40 s	
4	Infrared LEDs stimulation at 60°C for 100 s	$\%IRSL_{1.2\ s}/BOSL_{1s}$
5	Blue LEDs stimulation at 125°C for 100 s	$\%BOSL_{1s}$, $\%BOSL_F$, $\%BOSL_M$, $\%BOSL_S$
6	TL measurement up to 450°C	TL_{325pos} (°C)
7	Dose, 10 Gy	
8	TL measurement up to 450°C	$\%TL_{110°C}$ TL_{110pos} (°C)
9	TL measurement up to 450°C	TL background (°C)

(a)

(b)
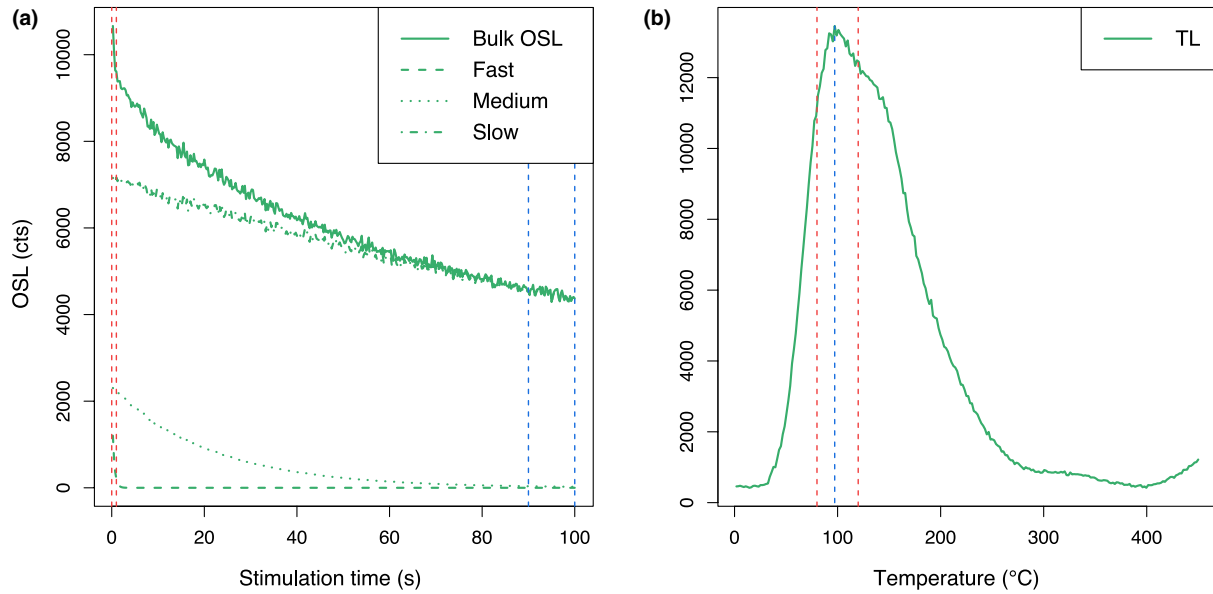
FIGURE 2 (a) Example of a deconvoluted OSL signal of an aliquot from sample BP133 of the Longá Formation. Red dashed lines show the integration interval of the signal. Blue dashed lines show the integrated interval used to calculate background. (b) Example of luminescence variables extracted from a TL curve of the same aliquot. Red dashed lines show the temperature interval (80–120°C) integrated for calculating the %TL$_{110°C}$ value and the blue dashed line marks the maximum TL intensity used also to estimate the temperature peak position (TL$_{110pos}$)

illumination conditions, the usefulness of the TL$_{325pos}$ is not compromised. Peak position was measured on the residual natural signal as it is not reproducible with the dosing and TL stimulations of steps 8 and 9. In total, eight luminescence signals were analysed: %BOSL$_{1s}$, % of fast OSL component (%BOSL$_F$), % of medium OSL component (%BOSL$_M$), % of slow OSL component (%BOSL$_S$), %IRSL$_{1.2\ s}$/BOSL$_{1s}$, %TL$_{110°C}$, TL$_{110pos}$ and TL$_{325pos}$.

$$\%\,BOSL_{1s} = \frac{BOSL_{[step\ 5;\ 0-1\ s]} - BOSL\,BG_{[step\ 5;\ 90-100\ s]}}{BOSL_{[step\ 5;\ 0-100\ s]} - BOSL\,BG_{[step\ 5;\ 90-100\ s]}} \times 100 \quad (2)$$

$$\%\,IRSL_{1.2s}/BOSL_{1s} = \frac{IRSL_{[step\ 4;\ 0-1.2\ s]} - IRSL\,BG_{[step\ 4;\ 90-100\ s]}}{BOSL_{[step\ 5;\ 0-1\ s]} - BOSL\,BG_{[step\ 5;\ 90-100\ s]}} \times 100 \quad (3)$$

$$\%\,TL_{110°C} = \frac{TL_{[step\ 8;\ 80-120°C]} - TL\,BG_{[step\ 9;\ 80-120°C]}}{TL_{[step\ 8;\ 0-450°C]} - TL\,BG_{[step\ 9;\ 0-450°C]}} \times 100 \quad (4)$$

To evaluate the influence of feldspar concentration in relation to quartz in the TL110°C peak we mounted synthetic aliquots of 20 grains with varied concentrations of potassium feldspar to quartz and plagioclase to quartz from 0 (100% quartz) to 20 grains of feldspar (0% quartz). The resulting TL curves allow to asses the feldspar influence in the varying %TL$_{110°C}$ (Figure S1).

The reproducibility of the luminescence signals was assessed by repeating the protocol from Table 1 on 10 aliquots from one sample of each unit. Standard errors relative

to the mean (RSE) were consistently below 10% for almost all samples and luminescence signals measured (Figure S2). The exceptions were the RSE for the %BOSL$_{1s}$ signal from samples BP139 (Piauí Formation) and for the medium OSL component contribution for samples BP210a (Pimenteiras Formation) and BP139 (Piauí Formation). The %IRSL$_{1.2s}$/BOSL$_{1s}$ signal yielded the higher RSE, with values up to 41% for sample BP174 (Cabeças Formation). On the other extreme, the TL$_{325pos}$ has relatively low RSE, with all values below 0.1%.

We also measured the sensitivity of modern sediment samples used by Sawakuchi et al. (2018) by applying the protocol from Table 1. Thus, it was possible to compare between the luminescence sensitivity of the studied samples and modern riverbed sediments sourced from tectonically active (Andes, Amazon River) and stable (Amazon craton, Xingu River) areas (Table S1 and Figure S3). The obtained results allow a direct comparison between our results and the luminescence sensitivities obtained by Sawakuchi et al. (2018), thus aiding interpretation of basin evolution based on modern source-to-sink sedimentary systems.

To assess whether there were statistically significant differences among stratigraphic units, we performed analysis of variance (ANOVA). A subsequent *t*-test comparing pairs of stratigraphic units allows us to detect which units contribute most to the differences observed using luminescence characteristics. For both statistical tests, we considered *p*-value <.05 as the significance level. Only *p*-values above this threshold will be discussed in further sections. For a quick visual evaluation of signal variation among samples,

we first plotted the kernel density estimations (KDE) for the main signals (%BOSL$_{1s}$, %TL$_{110°C}$, TL$_{110pos}$, TL$_{325pos}$ and %IRSL$_{1.2s}$/BOSL$_{1s}$). Data analysis was made using the R package "Luminescence" v0.9.11 (Kreutzer et al., 2012).

5 | RESULTS

Figure 3 shows examples of IRSL and OSL decay curves and TL glow curves for one aliquot from each studied stratigraphic unit. Samples with more intense IRSL signals (BP165, BP180, and BP64; Figure 3a) produce slow decaying OSL curves (Figure 3b) and TL glow curves with shoulders for temperature ranges between 80°C and 150°C (Figure 3d). The TL glow curves obtained after step 6 (Table 1) shows similar TL$_{325}$ peak positions among samples (Figure 3c) while the TL peak located at 110°C is only observed in TL glow curves obtained immediately after laboratory irradiation (Figure 3d) due to its inherent instability under room temperature. The low sensitivity of the TL$_{325}$ peak impeded reproducing this TL signal after the 10 Gy dose to regenerate the TL$_{110}$ peak.

Signal variation among samples can be observed from the KDE plot (Figure 4) for each stratigraphic unit. The OSL sensitivity values, expressed as %BOSL$_{1s}$, range between 5% and 25%, except for the Sambaíba Formation, which %BOSL$_{1s}$ values reach up to 32% (results by stratigraphic unit are in Table 2; results by sample are in Table S2). The %TL$_{110°C}$ presents values from 20% to 80%, with the Pimenteiras and Longá Formations showing %TL$_{110°C}$ values concentrated around ca. 30% and the Sambaíba Formation with values around 66%. The TL$_{110pos}$ values for all units are well clustered around $97 \pm 4°C$ while the TL$_{325pos}$ values have significant variation between 310°C and 345°C and their dispersion is sample dependent. The %IRSL$_{1.2s}$/BOSL$_{1s}$ values show great variability among stratigraphic units with minimum values of 0% found in the Sambaíba Formation and maximum values of 140%–150% in the Longá and Poti Formations.

The %BOSL$_{1s}$ values varied between 3% and 40%. An increase in BOSL$_{1s}$ occurs towards younger stratigraphic units ($p < .05$), especially for the Piauí, Motuca and Sambaíba Formations (Balsas Group), with the exception of the Cabeças Formation, which has a higher BOSL$_{1s}$
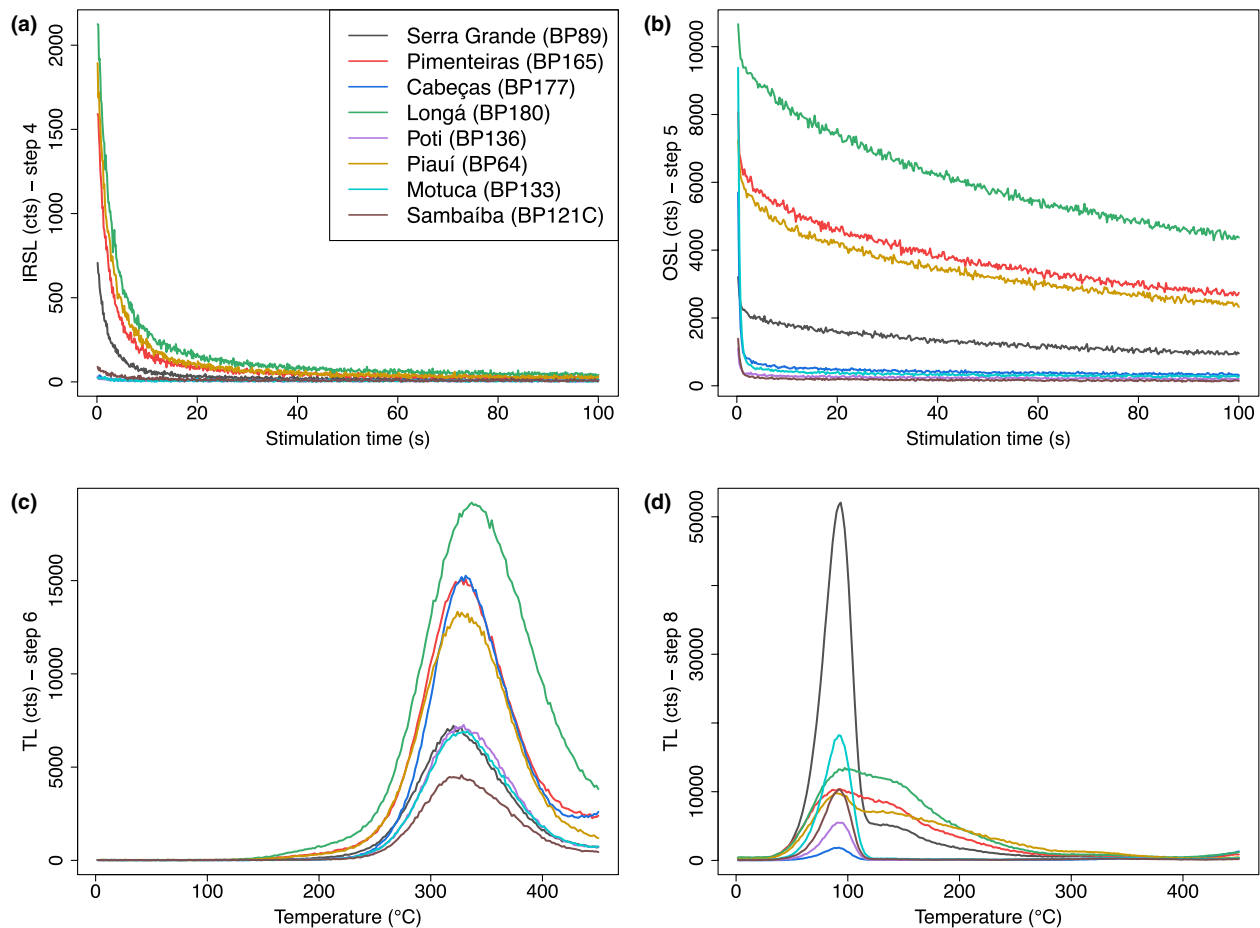

FIGURE 3 Variation in the shape of IRSL (a), OSL (b), natural TL (c) and regenerated TL (d) curves among the studied stratigraphic units (corresponding samples indicated in label of panel a). IRSL, OSL, natural TL and regenerated TL curves were obtained respectively after steps 4, 5, 6 and 8 from the protocol described in Table 1
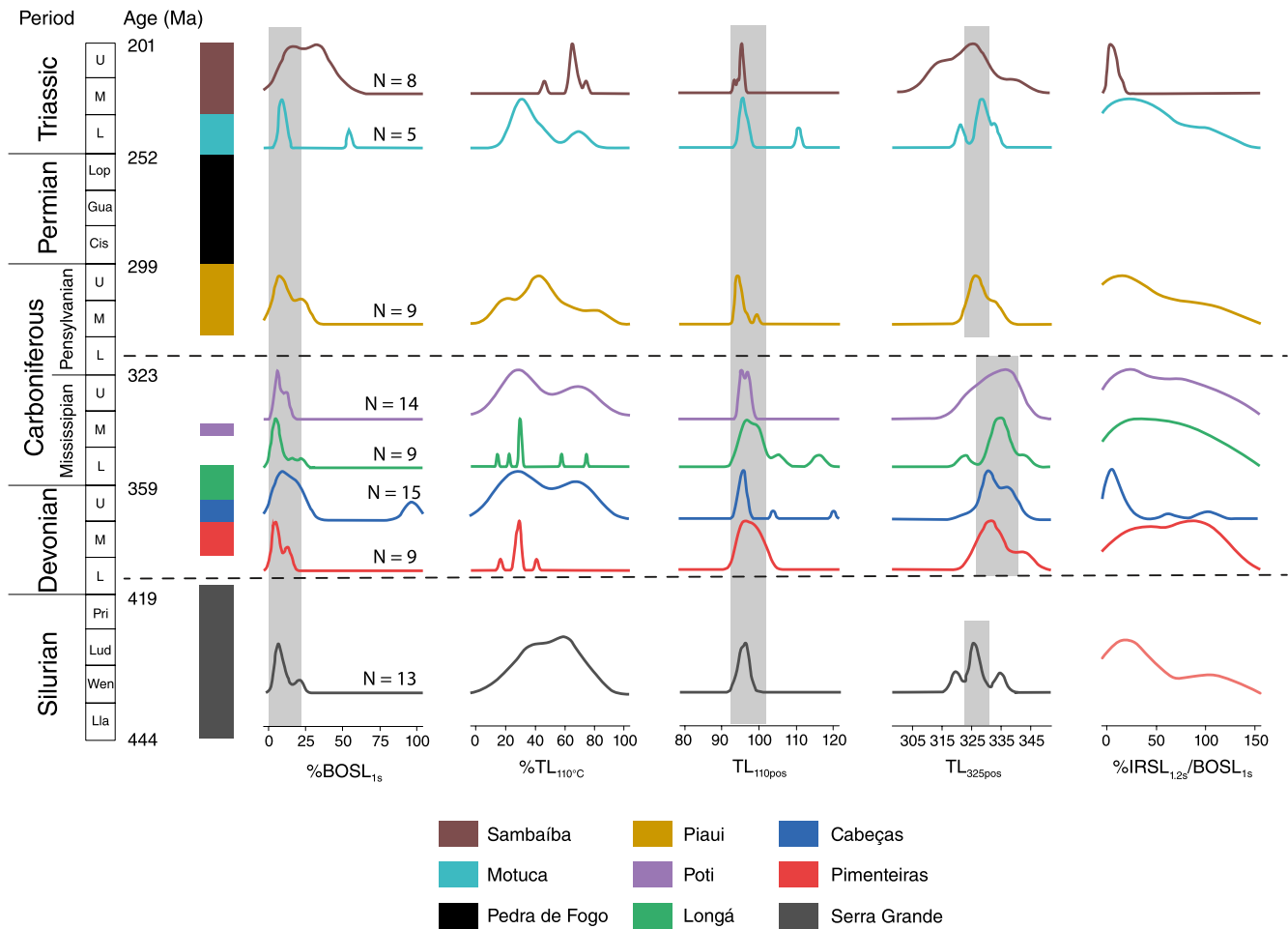
FIGURE 4   Kernel density estimation plots summarising the distributions of the main luminescence variables analysed in this study. Horizontal black dashed lines mark the position of the regional unconformities. Where possible, grey boxes illustrate the position of clustered density peaks. Chronostratigraphic chart based on Vaz et al. (2007)

compared with overlying units (Figure 5a,b). The deconvolution of OSL decay curves showed that the contribution of the $BOSL_F$ (Figure 5c,d) ranges from 20% to 50%, while the $BOSL_M$ (Figure 5e,f) is consistently uniform among all stratigraphic units, with a contribution of around 20%. The $BOSL_S$ (Figure 5g,h) inversely follows the $BOSL_F$ among stratigraphic units, decreasing its contribution from 50% in the older units to less than 30% in the younger units. Therefore, the OSL signals from the Serra Grande Group to the Motuca Formation are dominated by the slow OSL component, which represent up to 60% of the first second of light emission. For the Sambaíba Formation, the fast OSL component dominates the first second of light emission (56%), with the slow component contributing with 28%.

The $\%IRSL_{1.2s}/BOSL_{1s}$ shows a great variability between samples (Figure 6a) within stratigraphic units. For example, for the Cabeças Formation, $\%IRSL_{1.2s}/BOSL_{1s}$ values range between 0.1 (sample BP202; Table S2) to 108% (sample BP81a). At stratigraphic unit scale, the highest $\%IRSL_{1.2s}/BOSL_{1s}$ value correspond to the Pimenteiras Formation (64%) whereas the Sambaíba Formation yielded the lowest

value (6%). The $\%IRSL_{1.2\,s}/BOSL_{1s}$ values decrease with the increase in $\%BOSL_{1s}$ values, with values rising from the Serra Grande Group to the Pimenteiras, Longá and Potí Formations and reduced values are observed in the Sambaíba Formation (Figure 6a,b). As for the $\%BOSL_{1s}$, the Cabeças Formation also presents an anomalous behaviour in comparison with the rest of the stratigraphic units of the Canindé Group, with a $\%IRSL_{1.2s}/BOSL_{1s}$ value of 24%, while the other three formations from the Canindé Group yielded values close to 60%. In Figure 6c, clusters of samples are defined by the relationship between $\%BOSL_{1s}$ and $\%IRSL_{1.2s}/BOSL_{1s}$. This is exemplified by samples from the Pimenteiras Formation with low $\%BOSL_{1s}$ and variable $\%IRSL_{1.2s}/BOSL_{1s}$ or samples from the Sambaíba Formation with high $\%BOSL_{1s}$ and $\%IRSL_{1.2s}/BOSL_{1s}$ close to 0.

The $\%TL_{110°C}$ shows little variation across stratigraphic units in comparison with the $\%BOSL_{1s}$. The TL_{110} peak shows high sensitivity, with average up to 80% of the total TL glow curve (Figure 7a,b). The Serra Grande Group, Cabeças, Longá, Potí and Motuca Formations presented $\%TL_{110°C}$ values with high associated uncertainties (Figure 7)

TABLE 2 Summary of luminescence results for each stratigraphic unit. Errors correspond to one standard deviation. Results from individual samples are presented in Tables S1 and S2. Detailed measurement results and location of modern samples can be found in Figure S3

Stratigraphic unit	%$BOSL_{Is}$	% $BOSL_F$	% $BOSL_M$	% $BOSL_S$	%$IRSL_{1,2,s}$/$BOSL_{Is}$	%$TL_{110°C}$	TL_{110pos}	TL_{325pos}
Serra Grande $N = 13, n = 52$	9.2 ± 4.9	30.4 ± 13.8	19.0 ± 5.9	50.6 ± 12.9	45.9 ± 43.8	50.7 ± 17.3	95.5 ± 1.2	326.0 ± 4.7
Pimenteiras $N = 9, n = 36$	6.1 ± 3.8	20.1 ± 15.1	19.8 ± 2.9	60.0 ± 13.6	63.5 ± 38.8	29.6 ± 5.7	97.9 ± 2.5	333.7 ± 5.8
Cabeças $N = 15, n = 60$	18.4 ± 15.9	40.7 ± 18.8	18.6 ± 5.2	40.6 ± 18.0	23.6 ± 35.5	47.5 ± 21.2	97.8 ± 6.6	333.0 ± 4.6
Longá $N = 9, n = 36$	7.0 ± 5.3	28.2 ± 19.8	22.2 ± 7.9	47.0 ± 19.0	60.7 ± 46.9	36.3 ± 19.4	100.6 ± 6.5	334.3 ± 5.5
Potí $N = 14, n = 56$	8.2 ± 4.8	25.2 ± 13.6	19.4 ± 4.0	55.4 ± 11.6	61.1 ± 47.2	45.5 ± 21.2	96.3 ± 1.1	332.6 ± 6.3
Piauí $N = 9, n = 36$	11.7 ± 7.4	34.0 ± 16.8	19.7 ± 2.7	46.3 ± 17.3	47.4 ± 48.6	37.0 ± 10.2	95.1 ± 1.9	328.4 ± 3.7
Motuca $N = 5, n = 20$	13.8 ± 14.7	37.0 ± 16.8	18.2 ± 1.9	44.7 ± 16.0	41.1 ± 40.0	42.0 ± 17.5	98.8 ± 6.6	328.0 ± 4.3
Sambaíba $N = 8, n = 32$	23.5 ± 7.1	56.5 ± 8.7	15.8 ± 4.6	27.7 ± 10.0	6.2 ± 4.4	65.8 ± 7.1	95.2 ± 0.9	323.7 ± 8.7
Amazon River $N = 2, n = 8$	5.4 ± 3.0	23.1 ± 15.6	29.4 ± 29.1	54.3 ± 18.1	267.2 ± 135.2	25.4 ± 6.5	104.6 ± 5.1	352.6 ± 17.6
Xingu River $N = 2, n = 8$	71.8 ± 3.0	60.8 ± 16.9	37.6 ± 17.0	1.6 ± 0.4	0.6 ± 1.2	76.7 ± 6.4	108.0 ± 3.7	346.5 ± 9.2

Note: N is the number of samples; n is the number of aliquots.
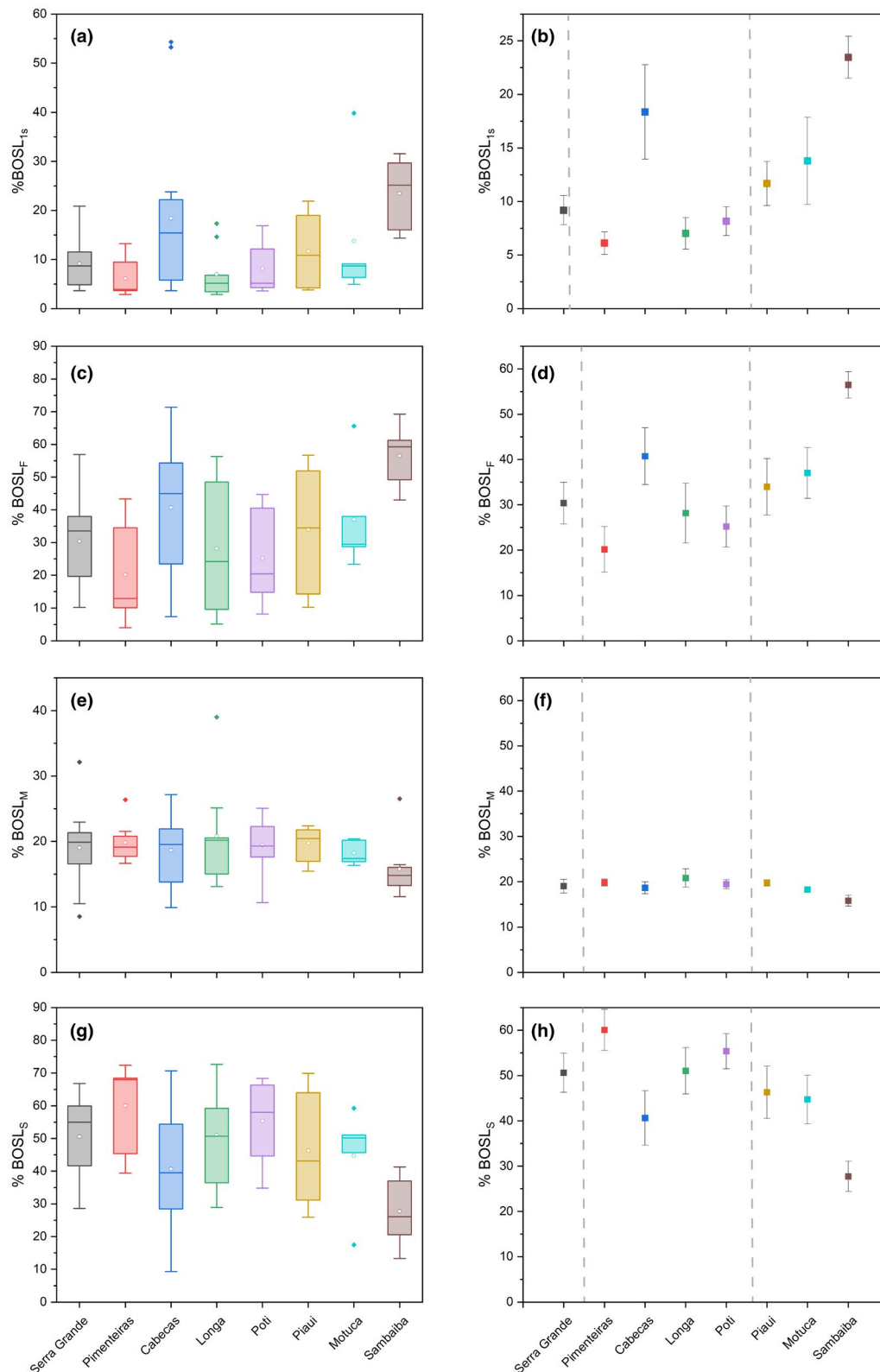
FIGURE 5 (a) Boxplots of %BOSL$_{1s}$ values including all samples organised by approximate age of each stratigraphic unit. (b) Mean %BOSL$_{1s}$ and standard error of each stratigraphic unit. Contribution of the % BOSL$_F$ (c, d), % BOSL$_M$ (e, f) and % BOSL$_S$ (g, h) for the initial second of light emission. Dashed gray lines indicate the position of the regional unconformities. In the boxplots, the dot and horizontal line inside the box respectively indicate the mean and the median. The upper and lower limits of the box indicate the first and third quartiles, respectively, while the upper and lower whiskers represent the 95th and the 5th percentiles, respectively. Dots beyond the whiskers represent outliers
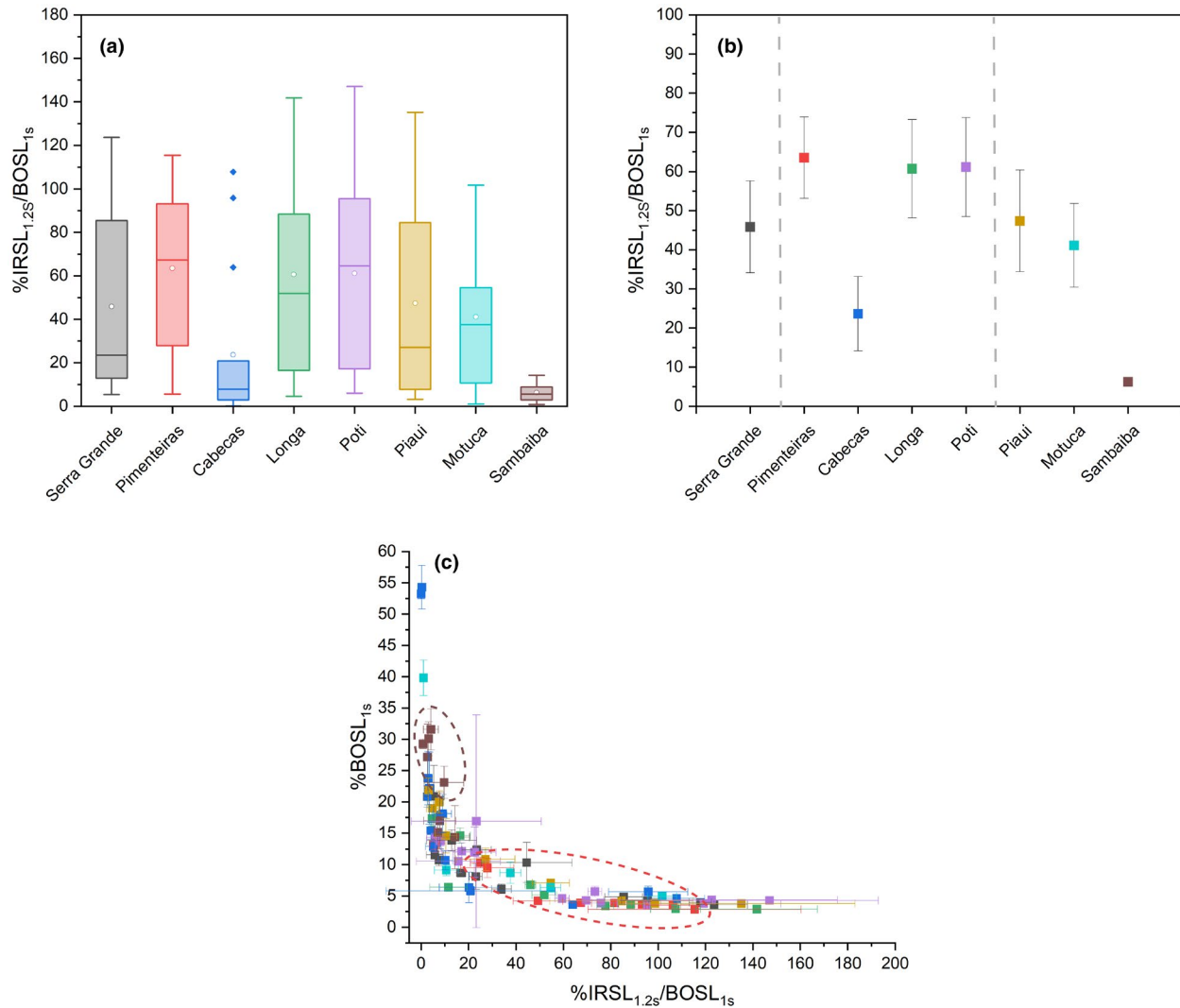
FIGURE 6 (a) Boxplot of the $\%IRSL_{1.2s}/BOSL_{1s}$ values for each stratigraphic unit. (b) Mean $\%IRSL_{1.2s}/BOSL_{1s}$ values and their corresponding standard errors for each stratigraphic unit. Dashed gray lines indicate the position of the regional unconformities. (c) Crossplot of $BOSL_{1s}$ and $\%IRSL_{1.2s}/BOSL_{1s}$ values. The dashed ellipses delimit samples from the Sambaíba (brown) and Pimenteiras (red) Formations. In the boxplots, the dot and horizontal line inside the box respectively indicate the mean and the median. The upper and lower limits of the box indicate the first and third quartiles, respectively, while the upper and lower whiskers represent the 95th and the 5th percentiles, respectively. Dots beyond the whiskers represent outliers

hindering the observation of variations across stratigraphy. The Pimenteiras Formation displays the lowest $\%TL_{110°C}$ sensitivity with values from 20% to 42% while the Sambaíba Formation yielded the highest $\%TL_{110°C}$ value with the lowest uncertainty (66 ± 7%). Apart from some outliers, the TL_{110pos} (Figure 7c,d) is located between 92°C and 108°C for most samples. The TL_{325pos} (Figure 7e,f) varies significantly among formations, allowing to distinguish two groups: (a) higher temperature peak position (>330°C) represented by the Pimenteiras, Cabeças, Longá and Potí Formations and (b) lower temperature group (<330°C) comprising the Serra Grande Group and the Piauí, Motuca and Sambaíba Formations (Figure 7e,f).

Almost all studied stratigraphic units presented significant differences between pairs of formations regarding their luminescence variables according to the ANOVA test results (Table S3). The exceptions are the $\%BOSL_M$ component ($p = .60$) and the TL_{110pos} value ($p = .06$). Comparisons between pairs of stratigraphic units showed that the Sambaíba Formation is mainly responsible for the p values under the significance level (T-test analysis, Table S4). We repeated the ANOVA test excluding the Sambaíba Formation to assess whether its higher $\%BOSF_{1s}$ was biasing the ANOVA results. Under this condition, the $\%BOSL_{1s}$ and the TL_{325pos} variables still yielded statistically significant differences for the studied stratigraphic units.
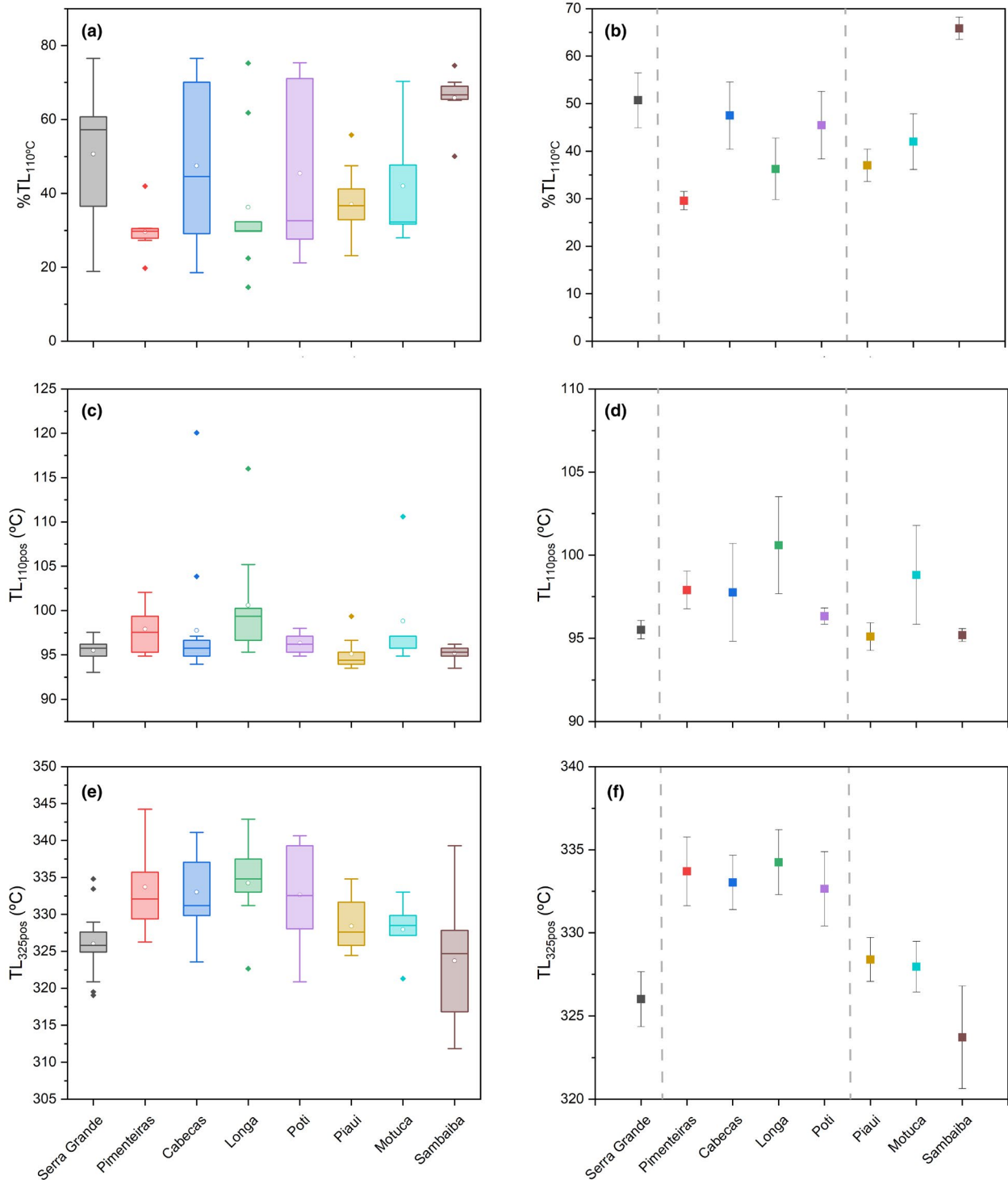
FIGURE 7 Variation of %$TL_{110°C}$ (a, b), TL_{110pos} (c, d) and TL_{325pos} (e, f) in the studied stratigraphic units. Data are represented by boxplots and means with their corresponding standard errors. Dashed gray lines indicate the position of the regional unconformities. In the boxplots, the dot and horizontal line inside the box respectively indicate the mean and the median. The upper and lower limits of the box indicate the first and third quartiles, respectively, while the upper and lower whiskers represent the 95th and the 5th percentiles, respectively. Dots beyond the whiskers represent outliers

The TL_{325pos} value yielded the highest number of pairs of stratigraphic units with statistically significant differences. It is noteworthy that for the TL_{325pos} value, significant differences between stratigraphic units appear to be controlled

by the position of unconformities (Figure 7f). As such, pairs of units from the Serra Grande and the Canindé Groups and pairs of units from the Canindé and Balsas Groups showed significant differences between them, while no statistical
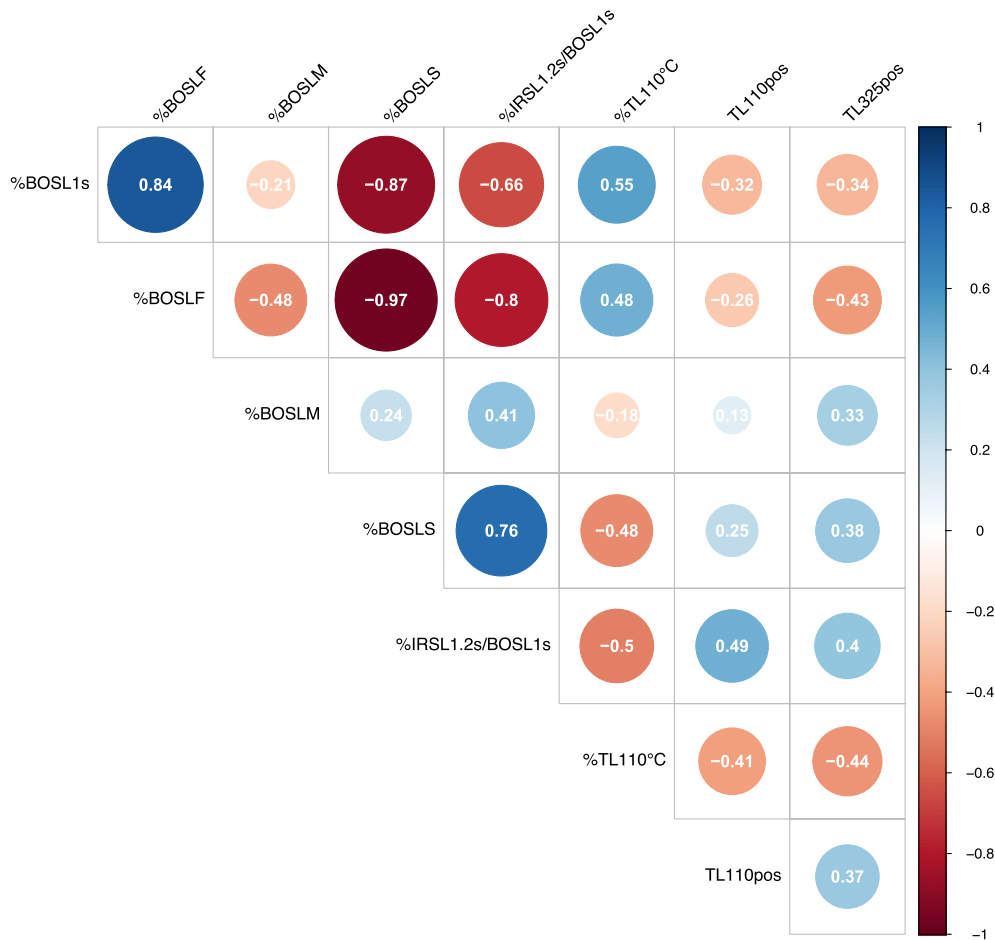
FIGURE 8 Correlation plot for all analysed luminescence signals. Values inside circles represent the R^2

differences were found between pairs of formations within the groups.

6 | DISCUSSION

6.1 | OSL and TL signals as proxies for discrimination of siliciclastic stratigraphic sequences

Luminescence sensitivity, represented by $\%BOSL_{1s}$, $\%BOSL_F$ and $\%BOSL_S$, and $\%IRSL_{1.2s}/BOSL_{1s}$ of the Parnaíba Basin stratigraphic units yielded statistically significant differences. The $\%BOSL_{1s}$ and $\%BOSL_F$ was calculated from OSL decay curve obtained after IRSL stimulation attempting to acquire an OSL signal dominated by quartz from polymineral aliquots. The $\%IRSL_{1.2s}/BOSL_{1s}$ value is probably related to the feldspar content of the sample (Duller, 2003). We also observed an inverse relationship between $\%IRSL_{1.2s}/BOSL_{1s}$ and $\%BOSL_{1s}$ values (Pearson's correlation coefficient of $-.66$, Figure 8), suggesting that feldspar content could affect $\%BOSL_{1s}$. In this case, the $\%BOSL_{1s}$ could not be exclusively

related to quartz OSL decay, if contribution from feldspar OSL signal is significant. However, measurements on pure quartz aliquots extracted from sediments with varied amount of feldspar grains showed lower $\%BOSL_{1s}$ in sediments with higher $\%IRSL_{1.2s}/BOSL_{1s}$ (Sawakuchi et al., 2018). This observation indicates a relationship between $\%BOSL_{1s}$, measured both in pure quartz or polymineral aliquots, and the mineralogical maturity of sediments, indicated by the feldspar content tracked by the $\%IRSL_{1.2s}/BOSL_{1s}$. This relationship would arise from the loss of feldspar grains and increase in quartz OSL sensitivity when sediments are progressively exposed to weathering in soils and transport in surface systems. Hence, weathering and break-up of grains during sediment transport reduce the relative amount of feldspar and promote the OSL sensitisation of quartz by cycles of burial irradiation and solar exposure (Pietsch et al., 2008). The relative contribution of the slow component to the OSL decay curve of quartz decreases with cycles of irradiation and illumination (Moska & Murray, 2006; Sawakuchi et al., 2011). Thus, the $\%BOSL_S$ would have inverse behaviour during sediment reworking when compared with the $\%BOSL_S$. As a conclusion, $\%IRSL_{1.2s}/BOSL_{1s}$ is a proxy for mineralogical

maturity of sediments while the $\%BOSL_{1s}$ indicates the degree of sediment reworking represented by burial irradiation-surface exposure cycles in soils or during sediment transport.

Previous studies demonstrated that the sensitivity of the $TL_{110°C}$ peak and fast OSL component of quartz, here indicated by the $\%BOSL_{1s}$, are correlated (Chen & Li, 2000; Stoneham & Stokes, 1991). However, $TL_{110°C}$ and the $\%BOSL_{1s}$ are weakly correlated (Pearson's correlation coefficient of .55) in the studied samples. In this study, TL was measured in polymineral aliquots. Then, it is possible that the variation in feldspar content in the studied samples may be inducing the observed scattering of $\%TL_{110°C}$ values due to partial overlapping of quartz and feldspar TL peaks in the 110°C region (Figure S1; Aitken, 1985).

While the TL_{110} peak position shows a narrow temperature range, located between 95°C and 100°C, and absence of significant variation among stratigraphic units (*p* value = .06), the TL_{325} peak position shows a significant stratigraphic trend, with intermediate temperature in the Serra Grande Group (327 ± 5°C), followed by a decrease from the Pimenteiras (334 ± 6°C) to the Sambaíba Formations (324 ± 9°C). Then, the TL_{325pos} can be used for stratigraphic discrimination at least at the scale of major stratigraphic boundaries, since the main differences are marked by the unconformities separating the Serra Grande, Canindé and Balsas Groups (Figure 7f). The stratigraphic variation of TL_{325} peak position appears similar to that observed for the $\%IRSL_{1.2 s}/BOSL_{1s}$ and $\%BOSL_{1s}$ values, which respectively indicate feldspar content and the sensitivity of fast OSL component of quartz. The TL peaks of quartz and feldspar overlap in the 300–350°C region when the emission is recorded in the UV (Aitken, 1985). Thus, the TL_{325pos} values would be influenced by feldspar content, similarly to the $\%IRSL_{1.2s}/BOSL_{1s}$ values, where sediments with lower feldspar concentration have lower temperature of the TL_{325pos}. However, the TL_{325pos} is more precise (lower RSE, Figure S2) discriminating between studied stratigraphic units in comparison with the $\%IRSL_{1.2s}/BOSL_{1s}$. Thus, both $\%IRSL_{1.2s}/BOSL_{1s}$ and TL_{325pos} would inform the feldspar content in the studied stratigraphic units. Based on this assumption, both signals show feldspar content decreasing progressively from the Pimenteiras Formation towards younger units. It is worth noting that feldspar content may be underestimated because the studied samples were collected in outcrops. Recent weathering or dissolution during diagenesis could influence the feldspar content, so the $\%IRSL_{1.2s}/BOSL_{1s}$ values should be interpreted with caution in terms of the surface conditions during sediment deposition. In any case, the TL_{325pos} value seems to provide valuable provenance information since it follows the inverse pattern of the $\%BOSL_{1s}$ and allows to discriminate between stratigraphic groups. Finally, the TL_{325pos} value is produced by a natural signal that remained even after preparing the samples in daylight and artificial light conditions, meaning that this signal could be obtained without requiring signal regeneration by a laboratory radiation source.

The studied stratigraphic units yield varied luminescence behaviour as demonstrated by OSL, IRSL and TL sensitivities, OSL fast component contribution and position of the TL_{325} peak. Such patterns of luminescence variation across stratigraphic units can be related to the mineralogical composition (namely relative content of feldspar) of sandstones, or to intrinsic luminescence characteristics of their quartz grains. Though the details of physical processes leading to these variations in luminescence properties are beyond of the scope of this investigation, the $\%BOSL_{1s}$ or TL_{325pos} values could be explored to discriminate siliciclastic stratigraphic units.

6.2 | Sediment source areas and recycling during basin filling

Though crystallisation conditions drive the primary OSL sensitivity of quartz in igneous and metamorphic source rocks (Guralnik et al., 2015; Sawakuchi et al., 2011), the sensitisation of quartz sediment grains during soil storage or sediment transport (Pietsch et al., 2008) surpasses the primary OSL sensitivity in several orders of magnitude (Mineli et al., 2021; Sawakuchi et al., 2011). Besides the sensitisation by illumination-irradiation cycles, the OSL sensitivity increases significantly when quartz is submitted to heating. However, the sensitisation by heating is only significant under temperatures above 500°C (Bøtter-Jensen et al., 1995), which is beyond the burial temperatures reached in sedimentary basins, including basins that experienced magmatic events, such as the Parnaíba Basin, because the thermal effect of emplaced magmatic bodies is spatially limited at basin scale (Da Silva et al., 2020). On the other hand, high radiation doses (>800 kGy) absorbed by quartz grains during long-term burial can hypothetically lead to luminescence desensitisation as observed by laboratory experiments (Autzen et al., 2018; Sawakuchi & Okuno, 2004). However, the $\%BOSL_{1s}$ values of the studied samples are close to sensitivity values from modern sediment samples (Sawakuchi et al., 2018), suggesting that any desensitisation during the long-term burial of the Parnaíba Basin sandstones is minor or absent. Therefore, the luminescence sensitivity of quartz grains from the studied stratigraphic units should mirror their sedimentary history, starting with the weathering and erosion of igneous or metamorphic source rocks and ending with final deposition cycle for burial in the Parnaíba Basin.

Previous provenance analysis based on detrital zircon geochronology and heavy mineral analyses point to the Araguaia Fold Belt at the west, the Tocantins Province at the south, and the Borborema Province at the east as primary sediment sources of the Parnaíba Basin (Hollanda et al., 2018).

Paleocurrents indicate a SW-NE transport trend at least for the Serra Grande Group and lower Canindé Group (Menzies et al., 2018), suggesting that the Araguaia Fold Belt would be the main sediment feeder during that time. However, the continuous presence of Neo-Mesoproterozoic ages from detrital zircons throughout the entire Parnaíba Basin stratigraphic sequence indicates that the Borborema Province was uplifted and eroded during the entire basin filling period (Hollanda et al., 2014). Detrital zircon geochronology and heavy mineral analysis point to a continuity of source areas with similar lithologies during the basin filling period, but the roundness of the studied zircons (Figure S4) increases for the Balsas Group in comparison with the Serra Grande and Canindé Groups. Thus, changes in source lithologies would play a minor role for the variation in luminescence characteristics during the Parnaíba Basin filling.

Organic and inorganic geochemical data of fine-grained rocks from the Serra Grande Group (Silurian) to the Motuca Formation (Late Permian) point that climate conditions changed from humid to arid in the western margin of the basin, while the eastern margin changed from arid to humid (Jaju et al., 2018). These opposite climate patterns could imply different conditions for source rock denudation and sediment transport across the basin, possibly leading to different luminescence characteristics of sedimentary units of the eastern and western margins of the Parnaíba Basin. However, the luminescence properties of units sampled in the western and eastern margins of the basin are similar (Figure S5), with major variations marked by regional unconformities separating the Serra Grande Group and the Pimenteiras Formation and the Poti and Piauí Formations. The most notable changes in $\%BOSL_{1s}$ and TL_{325pos} values (Figures 5b and 7b) coincides with regional erosive surfaces and climatic changes during the Early Devonian and Middle Carboniferous (Jaju et al., 2018). Hence, variation in luminescence characteristics would record temporal variations in sediment sourcing and transport in the Parnaíba Basin, being unsuitable to record climate gradients across the basin. The similarity of luminescence characteristics of sandy sediments accumulated in the eastern and western margins of the basin could also be related to the dominance of a specific source and decoupling between sources of fine-grained sediments (silt and clay) and sands. This occurs for example in the Amazon River Basin, where the fine-grained sediments are mostly supplied by specific areas of the Andes orogen (Höppner et al., 2018) while sands, especially quartz grains, have a relatively higher contribution from cratonic sources (Sawakuchi et al., 2018).

The OSL sensitivities obtained for the studied samples of the Parnaíba Basin are consistent with the sensitivity range reported for modern sediments of the Amazon Basin (Table 2), where higher (lower) OSL sensitivity sediments are derived from areas with lower (higher) denudation rates (Sawakuchi et al., 2018). Thus, continental-scale watersheds

such as the Amazon River Basin serve as analogue model on how luminescence properties of quartz and feldspar sand grains are tracking the sediment supply from source areas with contrasting climate and relief configuration. The inverse relationship between OSL sensitivity and denudation rate observed in the Amazon River Basin is attributed to source area lithologies, relief, and climate, which define sediment production rate, soil storage time, and erosion rate. High denudation rates (>70 m/Ma) are typical from the Andes Cordillera, an orogen feeding relatively young sediments to the Amazon River system mainly from erosion of Cenozoic igneous and metamorphic rocks, which supply sediments characterised by low (<10) $\%BOSL_{1s}$ values (Sawakuchi et al., 2018).

By contrast, the cratonic areas eastward of Andes are characterised by relatively low denudation rates (<30 m/Ma) and provide sediments derived from an assemblage of Pre-Cambrian metamorphic and igneous rocks and Paleozoic to Cenozoic sedimentary rocks, yielding $\%BOSL_{1s}$ values over 30 and up to 70% (Sawakuchi et al., 2018). Lower denudation rates of cratonic areas imply longer residence time of sediments in surface systems, favoring the reduction of feldspar content by weathering and the OSL sensitisation of quartz by burial and solar exposure cycles. Following the same rationale, the range of $\%BOSL_{1s}$ values found in the Parnaíba Basin sediments (Figure 5) would point to source areas with varied denudation rates, but with the dominance of source areas of high denudation rates typical of orogenic mountain ranges at least up to the Potí Formation deposition.

The $\%BOSL_{1s}$ values from the Piauí, Motuca and Sambaíba Formations (>10) suggest source areas with lower denudation rates such as a cratonic source or mixture of cratonic and orogenic sources (Sawakuchi et al., 2018). The eolian nature of the Sambaíba Formation might have had an additional effect on the OSL sensitivity, assuming that eolian systems with large dune fields usually have sediments supplied by fluvial or coastal systems, then, favoring a higher number of solar exposure-burial-exposure cycles and increased OSL sensitisation (Pietsch et al., 2008) before final deposition. Indeed, samples BP121a-h, all collected from a sandstone package within the Sambaíba Formation, show an increase in the $\%BOSL_{1s}$ values from older to younger sediment layers (Figure S6) that would record the increase in sediment recycling within the depositional system. Hence, the luminescence signals could also be used to track sediment recycling within specific sedimentary units, besides major landscape changes in sediment source areas. Despite depositional system types can contribute to quartz sensitisation and changes in mineralogical composition of sands, the major changes in $\%BOSL_{1s}$, $\%IRSL_{1.2s}/BOSL_{1s}$ and TL_{325pos} values coincides with the occurrence of regional erosional unconformities between the Serra Grande and Canindé Groups and between Canindé and Balsas Groups (Figures 5–7).

FIGURE 9 Relative contribution of high denudation rate sources (orange) and low denudation rate sources (blue) to the Parnaíba Basin sediments. Gray dashed lines represent the regional unconformities. The high denudation rate and low denudation rate end members sources are based on comparison to modern sediments of the Amazon River system derived from the Andes orogen and from Amazon craton in Brazil (Figure S3; Sawakuchi et al., 2018). Subsidence rates (Tozer et al., 2017) and major unconformities are shown for comparison
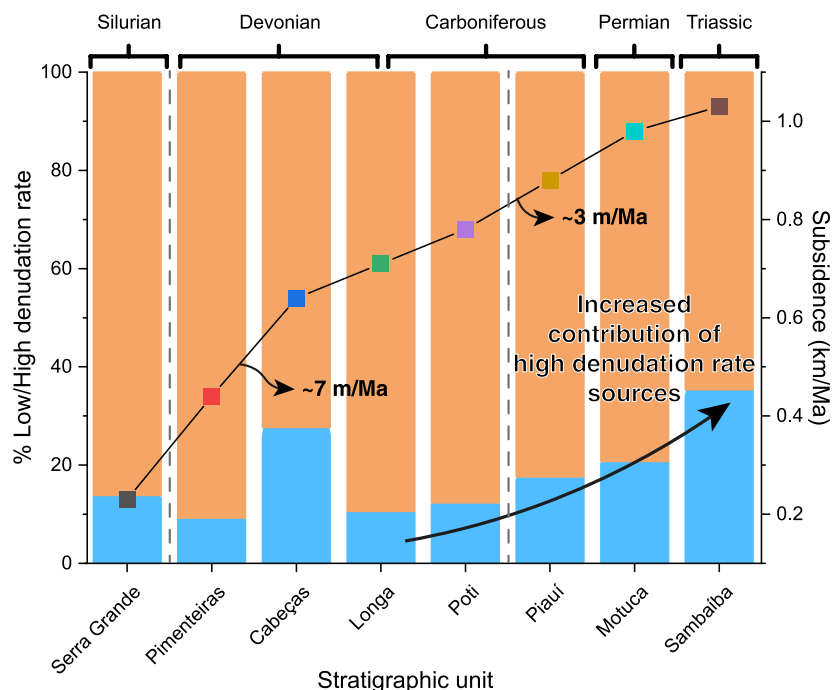
The outliers observed for some luminescence properties of samples from the Cabeças Formation (Figure 5) could be attributed to its varied depositional environments, with proximal (glacial and fluvial) to distal (deltaic and shallow marine) depositional systems (Figure 1b; Ponciano & Fávera, 2009). These diverse sedimentary environments could include proximal to distal sediment source areas with different denudations rates, thus explaining the large scattering of the luminescence properties of sands from this stratigraphic unit.

We can estimate the relative contribution of high denudation rate and low denudation rate sources to the Parnaíba Basin sediments considering the %BOSL$_{1s}$ from sands transported by modern rivers draining orogenic and cratonic regions. Thus, we used the %BOSL$_{1s}$ measured in selected sediment samples of the Amazon and Xingu Rivers (Table 2 and Table S1) respectively representing end members of high denudation rate (Andes orogen) and low denudation rate (Amazon craton) sources (Wittmann et al., 2011). It is important to note that orogenic and cratonic sources are differentiated based on their contrasting denudation rates imprinted by %BOSL$_{1s}$ of sediments (Sawakuchi et al., 2018). This allows the use of %BOSL$_{1s}$ values to decouple contributions of orogenic and cratonic sources for a given sediment mixture. Under this approach, the estimated contribution of sediments from orogenic (cratonic) sources varies from 86% (14%) in the Serra Grande Group to 65% (35%) in the Sambaíba Formation (Figure 9). When compared with the Parnaíba Basin subsidence rates (Tozer et al., 2017), a decreasing subsidence rate seems to be related to an increase in sediment sources with lower denudation rate. In fact, Tozer et al. (2017) estimated through backstripping analysis that ca. 70% of the total

subsidence occurred between the deposition of the Serra Grande Group (Early Silurian) and the Cabeças Formation (Late Devonian), while the remaining 30% of subsidence was accomplished between the Cabeças Formation (Late Devonian) and the Sambaíba Formation deposition (Late Triassic). This change in subsidence rate coincides with an increasing trend of the %BOSL$_{1s}$ values and a decreasing trend of the TL$_{325pos}$ values (Figure 9), especially during the deposition of the Balsas Group.

During the sedimentation of the Serra Grande and Canindé Groups, the basin maintained the same depositional axes and depocenter (Cunha, 1986; Góes et al., 1990; Mesner & Wooldrige, 1964). These axes overlapped the Transbrasiliano (NE-SW trend) and Picos-Santa Inês Lineaments (NW-SE trend coinciding with the Gurupi Belt) (Cunha, 1986). After the depositional cycle of the Canindé Group, the development of a regional unconformity eroded upper deposits of the Potí Formation. This unconformity is characterised by a 20 Ma depositional gap between the Mississippian and Pennsylvanian successions, which has been attributed to the Eohercynian Orogeny (Góes & Feijó, 1994; Vaz et al., 2007). With the return of sediment accumulation conditions, the basin configuration changed, with the closure of the connection with the eastward Amazonas Basin and the progressive migration of the depocenters to the west. Concurrently, depositional environments became increasingly continental in a warm and arid climate (Abrantes et al., 2019). The dry climax was the Sambaíba Desert recorded by the homonymous formation. This subsidence history punctuated by erosive phases points out that previously deposited units became cratonic sediment source areas and increased sedimentary recycling during basin filling. This would lead to the pattern

of higher %BOSL$_{1s}$, but lower feldspar content (%IRSL$_{1.2s}$/BOSL$_{1s}$) recorded by the younger stratigraphic units.

The progressive increase in %BOSL$_{1s}$ values (Figure 5b) supports increasing contribution of sediments from sources with lower denudation rate, analogous to modern cratonic settings, as well as higher sediment recycling during basin filling. The higher variability of %IRSL$_{1.2s}$/BOSL$_{1s}$ (Figure S2 and Figure 6) hinders the differentiation between stratigraphic units, but average %IRSL$_{1.2s}$/BOSL$_{1s}$ values suggest a decreasing feldspar content from older to younger stratigraphic units. The reduction in feldspar content matches with the decreasing contribution of high denudation rate source areas and long-term sediment recycling from the Serra Grande Group to the Sambaíba Formation. The decreasing contribution of sediments from high denudation sources suggested by the OSL sensitisation of quartz and dropping feldspar content from the Longá Formation (Late Devonian) to the Sambaíba (Early Triassic) Formation could be related to long-term changes in weathering conditions over continents. Besides climate and relief, chemical weathering and soil stability are highly dependent of the vegetation cover. In this case, the colonisation of continents by plants and further periods with expanded forests influenced weathering and sediment storage in source areas and continental depositional systems, creating conditions for longer residence of mineral grains in soils and surface sedimentary deposits. The Early Paleozoic units of the Parnaíba Basin, such as the Serra Grande Group, record pre-vegetation fluvial systems dominated by unstable bedload channels with faster sediment transport from sources to depositional sinks (Janikian et al., 2020). Appearance of vascular plants during the Devonian and latter diversification during the Pennsylvanian (Gibbling & Davies, 2012, and references therein) might have contributed to the impact on the weathering conditions and denudation rates of sediment source areas of the Parnaíba Basin during the Paleozoic. The use of %BOSL$_{1s}$ as proxy for long-term denudation rates in continents brings the possibility to explore interactions between sediment production, climate and plant evolution.

7 | CONCLUSIONS

The methodological approach presented here, until now performed only on Quaternary sediments, introduces a new way of analysing provenance of ancient sandstone formations based on luminescence signals of ubiquitous minerals and confirms its suitability for discriminating this type of rocks. Some additional advantages of this novel approach include minimised sample preparation, quick measurements (48 aliquots took approximately 12 hr), and low amount of sample needed (each aliquot contains approximately 8 mg of sample).

Luminescence signals from polymineral sand aliquots have great potential to discriminate major stratigraphic unconformities, especially the %BOSL$_{1s}$ or the relative proportion of fast (%BOSL$_F$) and slow (%BOSL$_S$) OSL components of quartz. The TL$_{325pos}$ measured from a natural TL signal and the %IRSL$_{1.2s}$/BOSL$_{1s}$ are additional stratigraphic markers. However, both luminescence characteristics may be related to the feldspar content, which can be influenced by an increased sedimentary recycling for younger units and by post-depositional diagenetic and late weathering processes biasing a primary (syn-depositional) stratigraphic signature.

Luminescence properties of quartz and feldspar sand grains are related to denudation rates in source areas and sediment recycling, allowing to track long-term landscape changes affecting the conditions of sediment supply for basin filling. Stratigraphic units with more heterogeneous OSL and TL sensitivity values point to larger sediment catchment areas. The variation in %BOSL$_{1s}$ values through stratigraphic units of the Parnaíba Basin suggests a decreasing contribution of sediments from high denudation rate source areas combined with an increasing sediment recycling from Late Devonian to Early Triassic. Using modern sediments as analogues of high denudation (orogenic) and low denudation (cratonic) sources, we interpret decreasing contribution of orogenic sources from the Serra Grande and Canindé Groups to the Balsas Group deposition. The increase in %BOSL$_{1s}$ from the Late Devonian (Longá Formation) to the Early Triassic (Sambaíba Formation) could be related long-term changes in sediment production and recycling resulted from shifts in relief, weathering, and storage of sediments in continents due to plant evolution since the Devonian.

CONFLICT OF INTEREST
The authors declare there are no conflicts of interest.

PEER REVIEW
The peer review history for this article is available at https://publons.com/publon/10.1111/bre.12590.

DATA AVAILABILITY STATEMENT
The data supporting the findings of this study are available from the corresponding author upon request.

ORCID

Ian del Río https://orcid.org/0000-0002-4782-5443
André O. Sawakuchi https://orcid.org/0000-0001-5016-2428
Ana M. Góes https://orcid.org/0000-0001-8575-1935
Maria Helena B. M. Hollanda https://orcid.org/0000-0003-2231-7917
Laura Y. Furukawa https://orcid.org/0000-0003-4024-3739
Naomi Porat https://orcid.org/0000-0002-5900-2460
Mayank Jain https://orcid.org/0000-0002-8942-7566
Thays D. Mineli https://orcid.org/0000-0002-3028-0192

REFERENCES

Abrantes, F. R. Jr, & Nogueira, A. C. R. (2013). Reconstituição paleoambiental das formações Motuca e Sambaíba, Permo-Triássico da Bacia do Parnaíba no sudoeste do Estado do Maranhão, Brasil. *Geologia USP Serie Cientifica*, *13*, 6–82. https://doi.org/10.5327/Z1519-874X201300030007

Abrantes, F. R. Jr, Nogueira, A. C. R., Andrade, L. S., Bandeira, J., Soares, J. L., & Medeiros, R. S. P. (2019). Register of increasing continentalization and palaeoenvironmental changes in the west-central Pangaea during the Permian-Triassic, Parnaíba Basin, Northern Brazil. *Journal of South American Earth Sciences*, *93*, 294–312. https://doi.org/10.1016/j.james.2019.05.006

Abrantes, F. R. Jr, Nogueira, A. C. R., & Soares, J. L. (2016). Permian paleogeography of west-central Pangea: Reconstruction using sabkha-type gypsum-bearing deposits of Parnaíba Basin, Northern Brazil. *Sedimentary Geology*, *341*, 175–188. https://doi.org/10.1016/j.sedgeo.2016.06.004

Agência Nacional do Petróleo, Gás e Biocombustíveis. (2021). *Boletim de Produção de Petróleo e Gás Natural*. http://www.anp.gov.br/arquivos/publicacoes/boletins-anp/producao/2020-06-boletim.pdf

Aitken, M. J. (1985). *Thermoluminescence dating* (359 pp.). Academic Press.

Aitken, M. J. (1998). *An introduction to optical dating*. Oxford University Press.

Angelim, L. A. A., Vasconcelos, A. M., Gomes, J. R. C., Wanderley, A. A., Forgiarini, L. & Medeiros, M. F. (2004). Folha Jaguaribe SB.24. In C. Schobbenhaus, J. H. Gonçalves, J. O. S. Santos, M. B. Abram, R. Leão Neto, G. M. M. Matos, R. M. Vidotti, M. A. B. Ramos & J. D. A. de Jesus (Eds.), *Carta Geológica do Brasil ao Milionésimo, Sistema de Informações Geográficas*. Programa Geologia do Brasil. CPRM, CD-ROM.

Araújo, R. N., Nogueira, A. C. R., Bandeira, J., & Angélica, R. S. (2016). Shallow lacustrine system of the Permian Pedra de Fogo Formation, Western Gondwana, Parnaíba Basin, Brazil. *Journal of South American Earth Sciences*, *67*, 57–70. https://doi.org/10.1016/j.jsames.2016.01.009

Autzen, M., Murray, A. S., Guérin, G., Baly, L., Ankjaergaard, C., Bailey, M., Jain, M., & Buylaert, J. P. (2018). Luminescence dosimetry: Does charge imbalance matter? *Radiation Measurements*, *120*, 16–32. https://doi.org/10.1016/j.radmeas.2018.08.001

Bailey, R. M. (2001). Towards a general kinetic model for optically and thermally stimulated luminescence of quartz. *Radiation Measurements*, *33*(1), 17–45. https://doi.org/10.1016/S1350-4487(00)00100-1

Blair, M. W., Yukihara, E. G., & McKeever, S. W. S. (2005). Experiences with single-aliquot OSL procedures using coarse-grain feldspars. *Radiation Measurements*, *39*, 361–374. https://doi.org/10.1016/j.radmeas.2004.05.008

Bøtter-Jensen, L., Agersnap Larsen, N., Mejdahl, V., Poolton, N. R., Morris, M. F., & McKeever, S. W. S. (1995). Luminescence sensitivity changes in quartz as a result of annealing. *Radiation Measurements*, *24*(4), 535–541. https://doi.org/10.1016/1350-4487(95)00006-Z

Bøtter-Jensen, L., McKeever, S. W., & Wintle, A. G. (2003). *Optically stimulated luminescence dosimetry* (1st ed.). Elsevier.

Campanha, V., & Rocha Campos, A. C. (1979). Alguns microfósseis da Formação Piauí (Neocarbonífero), Bacia do Parnaíba. *Boletim do Instituto de Geociências*, *10*, 57–67.

Chen, G., & Li, S. H. (2000). Studies of quartz 110 °C thermoluminescence peak sensitivity change and its relevance to optically stimulated luminescence dating. *Journal of Physics D: Applied Physics*, *33*(4), 437. https://doi.org/10.1088/0022-3727/33/4/318

Cisneros, J. C., Marsicano, C., Angielczyk, K. D., Smith, R. M. H., Richter, M., Fröbisch, J., Kammerer, C. F., & Sadleir, R. W. (2015). New Permian fauna from tropical Gondwana. *Nature Communications*, *6*, 8676. https://doi.org/10.1038/ncomms9676

Cordani, U. G., Brito Neves, B. B., Fuck, R. A., Porto, R., Thomaz Filho, A., & Cunha, F. M. B. (2009). Estudo preliminar de integração do Pré-Cambriano com os eventos tectônicos das bacias sedimentares brasileiras (Republicação). *Boletim de Geociências da Petrobras, Rio de Janeiro*, *17*(1), 133–204.

Cunha, F. M. B. (1986). *Evolução paleozoica da Bacia do Parnaíba e seu arcabouço tectônico* [Master thesis, Instituto de Geociências, Universidade Federal do Rio de Janeiro, Rio de Janeiro].

Da Silva, P. H. M., de Sá, E. F. J., de Souza, Z. S., & Córdoba, V. C. (2020). Structural controls and stratigraphic setting of sills: Example of the Central Atlantic Magmatic Province in the Parnaíba Basin, Northeast Brazil. *Journal of South American Earth Sciences*, *101*, 102606. https://doi.org/10.1016/j.jsames.2020.102606

Duller, G. A. T. (2003). Distinguishing quartz and feldspar in single grain luminescence measurements. *Radiation Measurements*, *37*(2), 161–165. https://doi.org/10.1016/S1350-4487(02)00170-1

Fedo, C. M., Sircombe, K. N., & Rainbird, R. H. (2003). Detrital zircon analysis of the sedimentary record. *Reviews in Mineralogy and Geochemistry*, *53*(1), 277–303. https://doi.org/10.2113/0530277

Giblling, M. R., & Davies, N. S. (2012). Palaeozoic landscapes shaped by plant evolution. *Nature Geoscience*, *5*, 99–105. https://doi.org/10.1038/ngeo1376

Góes, A. M., Coimbra, A. M., & Nogueira, A. C. R. (1997). Depósitos influenciados por tempestades e marés da Formação Potí (Carbonífero Inferior) da Bacia do Parnaíba. In M. L. Costa & R. Angélica (Orgs.), *Contribuições à geologia da Amazônia* (Vol. *1*, pp. 285–306). Sociedade Brasileira de Geologia-Núcleo Norte.

Góes, A. M., & Feijó, F. J. (1994). Bacia do Parnaíba. *Boletim de Geociências da Petrobras*, *8*(1), 57–67.

Góes, A. M., Rossetti, D. F., Nogueira, A. C. R., & Toledo, P. M. (1990). Modelo deposicional preliminar da Formação Pirabas no nordeste do Estado do Pará. *Boletim do Museu Paraense Emilio Goeldi. Série Ciências da Terra*, *2*, 3–15.

Góes, A. M. O., Travassos, W. A. S., & Nunes, K. C. (1993). *Projeto Parnaíba: Reavaliação e perspectivas exploratórias, paper presented at Relatorio Petrobras, DEXNOR-DINTER*.

Grahn, Y., & Caputo, M. V. (1992). Early Silurian glaciations in Brazil. *Palaeogeography, Palaeoclimatology, Palaeoecology*, *99*(1–2), 9–15. https://doi.org/10.1016/0031-0182(92)90003-N

Grahn, Y., Melo, J. H. G., & Steemans, P. (2005). Integrated chitinozoan and miospore zonation of the Serra Grande Group (Silurian-Lower

Devonian), Parnaíba Basin, Northeast Brazil. *Revista Española de Micropaleontología*, *37*(2), 183–204.

Grahn, Y., Young, C., & Borghi, L. (2008). Middle Devonian chitinozoan biostratigraphy and sedimentology in the eastern outcrop belt of the Parnaíba Basin, Northeastern Brazil. *Revista Brasileira de Paleontologia*, *11*(3), 137–146. https://doi.org/10.4072/rbp.2008.3.01

Gray, H. J., Jain, M., Sawakuchi, A. O., Mahan, S. A., & Tucker, G. E. (2019). Luminescence as a sediment tracer and provenance tool. *Reviews of Geophysics*, *57*, 987–1017. https://doi.org/10.1029/2019RG000646

Gray, H. J., Keen-Zebert, A., Furbish, D. J., Tucker, G. E., & Mahan, S. A. (2020). Depth-dependent soil mixing persists across climate zones. *Proceedings of the National Academy of Sciences of the United States of America*, *117*(16), 8750–8756. https://doi.org/10.1073/pnas.1914140117

Gray, H. J., Tucker, G. E., Mahan, S. A., McGuire, C., & Rhodes, R. (2017). On extracting sediment transport information from measurements of luminescence in river sediment. *Journal of Geophysical Research: Earth Surface*, *122*, 654–677. https://doi.org/10.1002/2016JF003858

Guralnik, B., Ankjaergaard, C., Jain, M., Murray, A. S., Müller, A., Wälle, M., Lowick, S. E., Preusser, F., Rhodes, E. J., Wu, T. S., Mathew, G., & Herman, F. (2015). OSL-thermochronometry using bedrock quartz: A note of caution. *Quaternary Geochronology*, *25*, 37–48. https://doi.org/10.1016/j.quageo.2014.09.001

Hollanda, M. H. B. M., Góes, A. M., & Negri, F. A. (2018). Provenance of sandstones in the Parnaíba Basin through detrital zircon geochronology. *Geological Society, London, Special Publications*, *472*, 181–197. https://doi.org/10.1144/SP472.16

Hollanda, M. H. B. M., Góes, A. M., Silva, D. B., & Negri, F. A. (2014). Proveniência sedimentar dos arenitos da Bacia do Parnaíba (NE do Brasil). *Boletim de Geociências da Petrobras*, *22*(2), 191–211.

Höppner, N., Lucassen, F., Chiessi, C. M., Sawakuchi, A. O., & Kasemann, S. A. (2018). Holocene provenance shift of suspended particulate matter in the Amazon River basin. *Quaternary Science Reviews*, *190*, 66–80. https://doi.org/10.1016/j.quascirev.2018.04.021

Huntley, D. J., & Lian, O. B. (2006). Some observations on tunnelling of trapped electrons in feldspars and their implications for optical dating. *Quaternary Science Reviews*, *25*(19–20), 2503–2512. https://doi.org/10.1016/j.quascirev.2005.05.011

Jain, M., & Ankjaergaard, C. (2011). Towards a non-fading signal in feldspar: Insight into charge transport and tunnelling from time-resolved optically stimulated luminescence. *Radiation Measurements*, *46*(3), 292–309. https://doi.org/10.1016/j.radmeas.2010.12.004

Jain, M., Murray, A. S., & Bøtter-Jensen, L. (2003). Characterization of blue-light stimulated luminescence components in different quartz samples: Implications for dose measurement. *Radiation Measurements*, *37*(4–5), 441–449. https://doi.org/10.1016/S1350-4487(03)00052-0

Jaju, M. M., Mort, H. P., Nader, F. H., Filho, M. L., & Macdonald, D. I. M. (2018). Palaeogeographical and palaeoclimatic evolution of the intracratonic Parnaíba Basin, NE Brazil using GPlates plate tectonic reconstructions and chemostratigraphic tools. *Geological Society, London, Special Publications*, *472*, 199–222. https://doi.org/10.1144/SP472.12

Janikian, L., de Almeida, R. P., Galeazzi, C. P., Tamura, L. N., Ardito, J. C., & Chamani, M. A. C. (2020). Variability of fluvial architecture in a poorly vegetated Earth: Silurian sheet-braided and meandering

ancestor river deposits recorded in northeastern Brazil. *Terra Nova*, *32*, 187–197. https://doi.org/10.1111/ter.12446

Kars, R. H., Wallinga, J., & Cohen, K. M. (2008). A new approach towards anomalous fading correction for feldspar IRSL dating—Tests on samples in field saturation. *Radiation Measurements*, *43*(2–6), 786–790. https://doi.org/10.1016/j.radmeas.2008.01.021

Kitis, G., Kiyak, N., Polymeris, G. S., & Tsirliganis, N. C. (2010). The correlation of fast OSL component with the TL peak at 325 °C in quartz of various origins. *Journal of Luminescence*, *130*(2), 298–303. https://doi.org/10.1016/j.jlumin.2009.09.006

Kreutzer, S., Burow, C., Dietze, M., Fuchs, M., Schmidt, C., Fischer, M., Friedrich, J., Mercier, N., Riedesel, S., Autzen, M., Mittelstrass, D., & Gray, H. (2021). *Luminescence: Comprehensive luminescence dating data analysis*. R package version 0.9.11. https://CRAN.R-project.org/package=Luminescence

Kreutzer, S., Schmidt, C., Fuchs, M. C., Dietze, M., Fischer, M., & Fuchs, M. (2012). Introducing an R package for luminescence dating analysis. *Ancient TL*, *30*(1), 1–8.

Loboziak, S., Steel, M., Caputo, M. V., & De Melo, J. H. G. (1992). Middle Devonian to lower Carboniferous miospore stratigraphy in the central Parnaíba Basin (Brazil). *Annales de la Société Géologique de Belgique*, *115*, 215–226.

Lü, T., & Sun, J. (2011). Luminescence sensitivities of quartz grains from eolian deposits in northern China and their implications for provenance. *Quaternary Research*, *76*, 181–189. https://doi.org/10.1016/j.yqres.2011.06.015

Medeiros, R. S. P. (2020). *O Pensilvaniano da Bacia do Parnaíba, Norte do Brasil: Implicações paleoambientais, paleoceanograficas e evolutivas para o Gondwana ocidental* (PhD thesis), Federal University of Pará.

Medeiros, R. S. P., Nogueira, A. C. R., Silva Junior, J. B. C., & Sial, A. N. (2019). Carbonate-clastic sedimentation in the Parnaiba Basin, northern Brazil: Record of carboniferous epeiric sea in the Western Gondwana. *Journal of American Earth Sciences*, *91*, 188–202. https://doi.org/10.1016/j.jsames.2019.01.018

Melo, J. H. G., & Loboziak, S. (2000). Viséan miospore biostratigraphy and correlation of the Poti Formation (Parnaíba Basin, northern Brazil). *Review of Palaeobotany and Palynology*, *112*, 147–165. https://doi.org/10.1016/S0034-6667(00)00043-9

Mendes, V. R., Sawakuchi, A. O., Chiessi, C. M., Giannini, P. C. F., Rehfeld, K., & Mulitza, S. (2019). Thermoluminescence and optically stimulated luminescence measured in marine sediments indicate precipitation changes over Northeastern Brazil. *Paleoceanography and Paleoclimatology*, *34*, 1476–1486. https://doi.org/10.1029/2019PA003691

Menzies, L. A., Carter, A., & Macdonald, D. I. M. (2018). Evolution of a cratonic basin: Insights from the stratal architecture and provenance history of the Parnaíba Basin. *Geological Society, London, Special Publications*, *472*, 157–179. https://doi.org/10.1144/SP472.18

Mesner, J. C., & Wooldrige, L. C. (1964). Maranhão Paleozoic Basin and Cretaceous Coastal Basins, Northern Brazil. *Bulletin of the American Association Petroleum Geologist*, *48*(9), 1475–1512.

Mineli, T. D., Sawakuchi, A. O., Guralnik, B., Lambert, R., Jain, M., Pupim, F. N., del Rio, I., Guedes, C. C. F., & Nogueira, L. (2021). Variation of luminescence sensitivity, characteristic dose and trap parameters of quartz from rocks and sediments. *Radiation Measurements*, *144*, 106583. https://doi.org/10.1016/j.radmeas.2021.106583

Morais-Neto, J. M., Hegarty, K. A., Karner, G. D., & Alkmin, F. F. (2009). Timing and mechanisms for the generation and modification

of the anomalous topography of the Borborema Province, north-eastern Brazil. *Marine and Petroleum Geology*, 26(7), 1070–1086. https://doi.org/10.1016/j.marpetgeo.2008.07.002

Morton, A., & Hallsworth, C. (1999). Processes controlling the composition of heavy mineral assemblages in sandstones. *Sedimentary Geology*, 124(1–4), 3–29. https://doi.org/10.1016/S0037-0738(98)00118-3

Moska, P., & Murray, A. S. (2006). Stability of the quartz fast-component in insensitive samples. *Radiation Measurements*, 41, 878–885. https://doi.org/10.1016/j.radmeas.2006.06.005

Murray, A. S., & Wintle, A. G. (2000). Luminescence dating of quartz using an improved single-aliquot regenerative-dose protocol. *Radiation Measurements*, 32(1), 57–73. https://doi.org/10.1016/S1350-4487(99)00253-X

Pietsch, T. J., Olley, J. M., & Nanson, G. C. (2008). Fluvial transport as a natural luminescence sensitizer of quartz. *Quaternary Geochronology*, 3(4), 365–376. https://doi.org/10.1016/j.quageo.2007.12.005

Ponciano, L. C. M. O., & Fávera, J. C. D. (2009). Flood dominated fluvio-deltaic system: A new depositional model for the Devonian Cabeças Formation, Parnaíba Basin, Piauí, Brazil. *Anais da Academia Brasileira de Ciências*, 81, 769–780. https://doi.org/10.1590/S0001-37652009000400014

Ponciano, L. C. M. O., Fonseca, V. M. M., & Machado, D. M. C. (2012). Taphofacies analysis of Late Early Givetian fossil assemblages of the Parnaíba Basin (State of Piauí, northeast Brazil). *Palaeogeography, Palaeoclimatology, Palaeoecology*, 326–328, 95–108. https://doi.org/10.1016/j.palaeo.2012.02.008

Preusser, F., Chithambo, M. L., Götte, T., Martini, M., Ranseyer, K., Sendezera, E. J., Susino, G. J., & Wintle, A. G. (2009). Quartz as a natural luminescence dosimeter. *Earth-Science Reviews*, 97, 184–214. https://doi.org/10.1016/j.earscirev.2009.09.006

Reimann, T., Román-Sánchez, A., Vanwalleghem, T., & Wallinga, J. (2017). Getting a grip on soil reworking – Single-grain feldspar luminescence as a novel tool to quantify soil reworking rates. *Quaternary Geochronology*, 42, 1–14. https://doi.org/10.1016/j.quageo.2017.07.002

Richetti, P. C., Schmitt, R. S., & Reeves, C. (2018). Dividing the South American continent to fit a Gondwana reconstruction: A model based on continental geology. *Tectonophysics*, 747–748, 79–98. https://doi.org/10.1016/j.tecto.2018.09.011

Rink, W. J., Rendell, H., Marseglia, E. A., Luff, B. J., & Townsend, P. D. (1993). Thermoluminescence spectra of igneous quartz and hydrothermal vein quartz. *Physics and Chemistry of Minerals*, 20, 353–361. https://doi.org/10.1007/BF00215106

Rossetti, D. F., Paz, J. D. S., & Góes, A. M. (2004). Facies analysis of the Codó formation (late Aptian) in the Grajaú area, southern São Luís-Grajaú Basin. *Anais da Academia Brasileira de Ciências*, 76, 791–806. https://doi.org/10.1590/S0001-37652004000400012

Sawakuchi, A. O., Blair, M. W., DeWitt, R., Faleiros, F. M., Hyppolito, T. N., & Guedes, C. C. F. (2011). Thermal history versus sedimentary history: OSL sensitivity of single quartz grains extracted from igneous and metamorphic rocks and sediments. *Quaternary Geochronology*, 6(2), 261–272. https://doi.org/10.1016/j.quageo.2010.11.002

Sawakuchi, A. O., Jain, M., Mineli, T. D., Nogueira, L., Bertassoli, D. J. Jr, Häggi, C., Sawakuchi, H. O., Pupim, F. N., Grohmann, C. H., Chiessi, C. M., Zabel, M., Mulitza, S., Mazoca, C. E. M., & Cunha, D. F. (2018). Luminescence of quartz and feldspar finger-prints provenance and correlates with the source area denudation in the Amazon River basin. *Earth and Planetary Science Letters*, 492, 152–162. https://doi.org/10.1016/J.EPSL.2018.04.006

Sawakuchi, A. O., Rodrigues, F. C. G., Mineli, T. D., Mendes, V. R., Melo, D. B., Chiessi, C. M., & Giannini, P. C. F. (2020). Optically stimulated luminescence sensitivity of quartz for provenance analysis. *Methods and Protocols*, 3(1), 6. https://doi.org/10.3390/mps3010006

Sawakuchi, G. O., & Okuno, E. (2004). Effects of high gamma ray doses in quartz. *Nuclear Instruments and Methods in Physics Research Section B: Beam Interactions with Materials and Atoms*, 218, 217–222. https://doi.org/10.1016/j.nimb.2003.12.021

Singarayer, J. S., & Bailey, R. M. (2003). Further investigations of the quartz optically stimulated luminescence components using linear modulation. *Radiation Measurements*, 37(4–5), 451–458. https://doi.org/10.1016/S1350-4487(03)00062-3

Singarayer, J. S., Bailey, R. M., Ward, S., & Stokes, S. (2005). Assessing the completeness of optical resetting of quartz OSL in the natural environment. *Radiation Measurements*, 40(1), 13–25. https://doi.org/10.1016/j.radmeas.2005.02.005

Spooner, N. A., Prescott, J. R., & Hutton, J. T. (1988). The effect of illumination wavelength on the bleaching of the thermoluminescence (TL) of quartz. *Quaternary Science Reviews*, 7(3–4), 325–329. https://doi.org/10.1016/0277-3791(88)90023-6

Spooner, N. A., & Questiaux, D. G. (2000). Kinetics of red, blue and UV thermoluminescence and optically-stimulated luminescence from quartz. *Radiation Measurements*, 32(5–6), 659–666. https://doi.org/10.1016/S1350-4487(00)00067-6

Stoneham, D., & Stokes, S. (1991). An investigation of the relationship between the 110 °C TL peak and optically stimulated luminescence in sedimentary quartz. *International Journal of Radiation Applications and Instrumentation. Part D. Nuclear Tracks and Radiation Measurements*, 18(1–2), 119–123. https://doi.org/10.1016/1359-0189(91)90102-N

Thomsen, K. J., Murray, A. S., & Bøtter-Jensen, L. (2011). Stability of IRSL signals from sedimentary K-feldspar samples. *Geochronometria*, 38(1), 1–13. https://doi.org/10.2478/s13386-011-0003-z

Thomsen, K. J., Murray, A. S., Jain, M., & Bøtter-Jensen, L. (2008). Laboratory fading rates of various luminescence signals from feldspar-rich sediment extracts. *Radiation Measurements*, 43(9–10), 1474–1486. https://doi.org/10.1016/j.radmeas.2008.06.002

Tozer, B., Watts, A. B., & Daly, M. C. (2017). Crustal structure, gravity anomalies, and subsidence history of the Parnaíba cratonic basin, Northeast Brazil. *Journal of Geophysical Research: Solid Earth*, 122, 5591–5621. https://doi.org/10.1002/2017JB014348

Valla, P. G., Lowick, S. E., Herman, F., Champagnac, J. D., Steer, P., & Guralnik, B. (2016). Exploring $IRSL_{50}$ fading variability in bedrock feldspars and implications for OSL thermochronometry. *Quaternary Geochronology*, 36, 55–66. https://doi.org/10.1016/j.quageo.2016.08.004

Vasconcelos, A. M., Ribeiro, J. A. P., Colares, J. Q. S., Gomes, I. P., & Forgiarini, L. L. (2004). Folha Teresina SB.23. In C. Schobbenhaus, J. H. Gonçalves, J. O. S. Santos, M. B. Abram, R. Leão Neto, G. M. M. Matos, R. M. Vidotti, M. A. B. Ramos, & J. D. A. de Jesus (Eds.), *Carta Geológica do Brasil ao Milionésimo, Sistema de Informações Geográficas*. Programa Geologia do Brasil. CPRM, CD-ROM.

Vaz, P. T., Rezende, N. G. A. M., Wanderley Filho, J. R., & Travassos, W. A. S. (2007). Bacia do Parnaíba. *Boletim de Geociências da Petrobras*, 15, 253–263.

Vieira, L. V., & Scherer, C. M. D. (2017). Facies architecture and high-resolution sequence stratigraphy of an aeolian, fluvial and shallow marine system in the Pennsylvanian Piauí Formation, Parnaíba

Basin, Brazil. *Journal of South American Earth Sciences*, *76*, 238–256. https://doi.org/10.1016/j.jsames.2017.03.009

Wintle, A. G., & Adamiec, G. (2017). Optically stimulated luminescence signals from quartz: A review. *Radiation Measurements*, *98*, 10–33. https://doi.org/10.1016/j.radmeas.2017.02.003

Wintle, A. G., & Murray, A. S. (1997). The relationship between quartz thermoluminescence, photo-transferred thermoluminescence, and optically stimulated luminescence. *Radiation Measurements*, *27*(4), 611–624. https://doi.org/10.1016/S1350-4487(97)00018-8

Wittmann, H., von Blanckenburg, F., Maurice, L., Guyot, L., Filizola, N., & Kubik, P. W. (2011). Sediment production and delivery in the Amazon River basin quantified by in situ-produced cosmogenic nuclides and recent river loads. *Geological Society of America Bulletin*, *123*, 934–950. https://doi.org/10.1130/B30317.1

Zular, A., Sawakuchi, A. O., Guedes, C. C. F., & Giannini, P. C. F. (2015). Attaining provenance proxies from OSL and TL sensitivities: Coupling with grain size and heavy minerals data from southern Brazilian coastal sediments. *Radiation Measurements*, *81*, 39–45. https://doi.org/10.1016/j.radmeas.2015.04.010

SUPPORTING INFORMATION

Additional Supporting Information may be found online in the Supporting Information section.